Advanced Review

Reaction path Hamiltonian and the unified reaction valley approach

Elfi Kraka*

One of the major goals of chemistry is to control chemical reactions with the purpose of generating new compounds with useful properties. Control of a chemical reaction implies a detailed understanding of its mechanism as it results from the breaking and forming of chemical bonds. In practice, it is rather difficult to get a detailed mechanistic and dynamical description of even the simplest chemical reactions. This has to do with the fact that apart from reactants, products, and possible stable intermediates, all other molecular forms encountered during a reaction have such a short lifetime that standard experimental means are not sufficient to detect and describe them. Progress in modern laser spectroscopy seems to provide an access to transient species with lifetimes in the pico- to femtosecond region; however, computational investigations utilizing state-of-the art methods of quantum chemistry, in particular *ab initio* methods, provide still the major source of knowledge on reaction mechanism and reaction dynamics. The reaction path Hamiltonian model has proven as a powerful tool to derive the dynamics of a chemical reaction by following the reacting species along the reaction path from reactants to products as traced out on the potential energy surface. In this article, the original reaction path Hamiltonian will be reviewed, extensions and applications over the past decades will be summarized, and a new perspective, namely to use it in form of the unified reaction valley approach to derive a deep and systematic insight into the mechanism of a chemical reaction will be introduced. *WIREs Comput Mol Sci* 2011 1 531–556 DOI: 10.1002/wcms.65

INTRODUCTION

One of chemistry's major objectives is the control of chemical reactions. Only by control of a chemical reaction can it be guaranteed that products with desirable properties rather than unwanted side products are generated. Control of chemical reactions starts with the understanding of the reaction mechanism, the knowledge of the activation energies (enthalpies) and, directly related to the latter, the knowledge of reaction rate constants. For a century, chemists have measured rate constants and activation enthalpies (or Arrhenius activation energies) to learn about the properties of chemical reactions with the goal of controlling them. Quantum chemical methods have added substantially to this knowledge by calculating reaction energies and barriers, describing the properties of transition states and reaction intermediates or calculating directly reaction rates by using appropriate dynamics methods.[1]

The potential energy surface (PES) is one of the most important concepts in chemistry[2] in the application of electronic structure methods to the study of molecular structures, properties, mechanism, and dynamics. Once the PES is known for a reacting system, one can apply Newton dynamics to calculate the movements of the reaction complex (the assembly of the reacting molecules and/or atoms) on the PES and to determine reaction rates and other related dynamic properties. However, even with today's computer technology the calculation of a PES for a larger reacting system provides a formidable task.[3] Fortunately not all locations on a PES are of equal importance for a chemical reaction. Miller et al.[4] introduced in 1980 the reaction path Hamiltonian (RPH) concept that allows the derivation of reasonable rate constants, energy distributions, and mechanistic information by concentrating on a smaller portion of the whole PES, namely the reaction path region, connecting reactants, transition state, and products. In the same year, Kato and Morokuma[5] suggested to

*Correspondence to: ekraka@gmail.com

Department of Chemistry, Southern Methodist University, Dallas, TX, USA

DOI: 10.1002/wcms.65

discuss the mechanism of energy disposal along the reaction pathway in relation to the characteristic features of PES. They introduced a simplified theoretical model being defined in terms of a reaction path (RP) and the normal coordinates perpendicular to the motion along the path.

Since then, the RPH concept has been frequently used for the study of reaction dynamics, while its potential with the regard to the study of reaction mechanisms has not yet fully been exploited.[6,7]

The article is structured in the following way: (1) the original RPH of Miller et al. will be described, (2) extensions of the original RPH will be summarized, and (3) the application of the RPH to elucidate the mechanisms of chemical reactions in full detail will be introduced.

THE REACTION PATH HAMILTONIAN

Miller et al.[4] derived the classical RPH for a reacting molecular system (reaction complex), combining the early ideas of Hofacker[8] and Marcus,[9–11] the intrinsic reaction coordinate (IRC) path of Fukui,[12] and the large amplitude model of Hougen et al.[13] Essential to their derivation was the idea of a reaction valley as the location where all important mechanistic and dynamic steps of a chemical reaction take place. Considering a reaction complex with K atoms and (3K-L) internal coordinates, (L is the number of overall translations and external rotations of the reaction complex, $L = 6$ for a nonlinear, $L = 5$ for a linear reaction complex), the (3K-L) dimensional configuration space of the RPH is partitioned into the one-dimensional (1D) reaction coordinate s (describing the motion along the valley floor) and the (3K-L-1) dimensional reaction valley (describing the valley walls) perpendicular to s. The reaction valley at each path point s is defined by the curvature of the valley floor in directions perpendicular to the RP. Considering that for a fixed value of s the potential energy $V(\mathbf{R})$, (with $\mathbf{R} = 1,2,\ldots,$ 3K-L), is a minimum in the (3K-L-1)-dimensional subspace orthogonal to the RP subspace and expanding $V(\mathbf{R})$ up to second-order (harmonic valley assumption), the curvatures of the valley and, by this, its steepness can be calculated in the same way as done for a minimum in the full space. The only difference is that the Hessian (force constant) matrix at point s is expressed now in mass-weighted coordinates and constructed by projecting out not only rotations and translations of the reaction complex but also its translational motion along the RP thus yielding the mass-weighted projected force constant matrix $\mathbf{K}(s)$[4]:

$$\mathbf{K}(s) = [\mathbf{I} - \mathbf{P}(s)]^{+}\mathbf{F}^{x}(s)[\mathbf{I} - \mathbf{P}(s)], \tag{1}$$

where $[\mathbf{I} - \mathbf{P}(s)]$ is a projector onto the (3K-L-1)-dimensional subspace and $\mathbf{F}^{x}(s)$ is the mass-weighted Cartesian force constant matrix. By diagonalizing, i.e., solving the vibrational eigenvalue problem, Equation (2)

$$\mathbf{K}(s)\,\mathbf{l}_{\mu}(s) = \omega_{\mu}^{2}(s)\,\mathbf{l}_{\mu}(s) \tag{2}$$

the 3K-L-1 mass-weighted generalized normal modes $\mathbf{l}_{\mu}(s)$, normal coordinates $Q_{\mu}(s)$, which measure the displacements along the directions of $\mathbf{l}_{\mu}(s)$, and the associated frequencies $\omega_{\mu}(s)$ are obtained. $(L + 1)$ frequencies corresponding to translations, rotations, and the motion along the RP are equal to zero because of Equation (1). The generalized normal mode vectors are orthogonal to the RP and span the (3K-L-1)-dimensional subspace of the reaction valley. Hence, the normal mode coordinates $Q_{\mu}(s)$ are perfectly suited as valley coordinates. The frequencies $\omega_{\mu}(s)$ describe the curvature and the steepness of the valley walls in the 3K-L-1 directions. Large frequencies indicate steep energy walls, whereas small frequencies describe a flat valley with only slowly increasing energy walls. Each point $\mathbf{x}i$ in mass-weighted Cartesian coordinate space is given by

$$\mathbf{x}_{i} = \mathbf{x}_{i}(s) + \sum_{\mu}^{\text{3K-L-1}} \mathbf{l}_{\mu,i}(s)\,Q_{\mu}(s) \tag{3}$$

i.e., as a linear combination of the path coordinate $\mathbf{x}_{i}(s)$ and the orthogonal valley coordinates.

The original RPH of Miller et al.[4] is a classical Hamiltonian. It is based on Fukui's IRC path,[12] the steepest descent path in mass-weighted Cartesian coordinates. The reaction valley is assumed to be harmonic, e.g., it can be fully described with the help of the mass-weighted projected force constant matrix $\mathbf{K}(s)$ evaluated at each path point of interest. This assumption is justified as long as the relevant reaction dynamics takes place close to the reaction path. To further simplify the RPH, most applications exclude rotations of the reaction complex in three-dimensional (3D) space by assuming zero angular momentum ($\mathbf{J} = 0$), e.g., the RPH s contains neither a rotational part nor rotational–vibrational coupling terms. A discussion of the RPH for $J > 0$ can be found in Miller et al.[4]; see also below.

Considering Equation (3), the RPH adopts the form of Equation (4): [4]

$$H[s, p_s, \{Q_{\mu}\}\{P_{\mu}\}] = T\,[s, p_s, \{Q_{\mu}\}\{P_{\mu}\}] + V\,[s, \{Q_{\mu}\}], \tag{4}$$

where $(s, \{Q_\mu\})$ are the reaction valley coordinates and $(p_s, \{P_\mu\})$ their conjugated momenta. The potential $V[s, \{Q_\mu\}]$ is approximated at each point s by the potential $V_o(s)$ at s plus the potential for harmonic displacements perpendicular to the path:

$$V[s, \{Q_\mu\}] = V_o(s) + \frac{1}{2} \sum_{\mu}^{3K\text{-}L\text{-}1} \omega_\mu^2(s)\, Q_\mu^2(s). \quad (5a)$$

The kinetic energy (for zero total angular momentum) is given by Equation (5b):

$$T[s, p_s, \{Q_\mu\}\{P_\mu\}] = \frac{1}{2} \frac{\left[p_s - \sum_{\mu}^{3K\text{-}L\text{-}1} \sum_{\nu} B_{\mu,\nu}(s)\, Q_\mu(s) P_\nu(s)\right]^2}{\left[1 + \sum_{\mu}^{3K\text{-}L\text{-}1} B_{\mu,s}(s)\, Q_\mu(s)\right]^2} + \frac{1}{2} \sum_{\mu}^{3K\text{-}L\text{-}1} P_\mu^2(s). \quad (5b)$$

The first term corresponds to the kinetic energy part of the movement along the RP including coupling terms between RP and transverse motions. The second term represents the kinetic energy part associated with a movement orthogonal to the path direction.

The coupling terms $B_{\mu,\nu}(s)$ are given by the dot product between the normal mode vector $\mathbf{l}_\nu(s)$ and the change of normal mode vector $\mathbf{l}_\mu(s)$: [4,14]

$$B_{\mu,\nu}(s) = \{\mathbf{l}_\nu(s)\}^+ \frac{d\mathbf{l}_\mu(s)}{ds} = -B_{\nu,\mu}(s). \quad (6)$$

The $B_{\mu,\nu}(s)$ coefficients describe the mixing between modes μ and ν induced by the motion of the reaction complex along the RP. As this motion involves a rotation of the vibrational modes about the RP, the $B_{\mu,\nu}(s)$ terms are referred to as mode–mode or *Coriolis* coupling *s*.

The terms $B_{\mu,s}(s)$ are given as the dot product between the reaction path vector $\mathbf{t}(s)$ and the change of the normal mode vector $\mathbf{l}_\mu(s)$ or the dot product of normal vector $\mathbf{l}_\mu(s)$ and the reaction path curvature vector $k(s)$ [4,14]

$$B_{\mu,s}(s) = \{\mathbf{t}(s)\}^+ \frac{d\mathbf{l}_\nu(s)}{ds} = -\{\mathbf{l}_\mu(s)\}^+ \frac{d\mathbf{t}(s)}{ds} = -\{\mathbf{l}_\mu(s)\}^+ \mathbf{k}(s) \quad (7)$$

with

$$\mathbf{t}(s) = \frac{d\mathbf{x}(s)}{ds}.$$

They describe the dynamic coupling between the RP and vibrational mode $\mathbf{l}_\mu(s)$, e.g., the mixing between the motion along the RP and the vibrational motion in mode μ induced by the curvature of the RP in the (3K-L)-dimensional space. As $B_{\mu,s}(s)$ becomes larger, the mixing between the RP and vibrational mode μ increases and energy transfer from translation to vibration and vice versa becomes more and more facile.[7] The scalar curvature $k(s)$of the RP is defined as [4,14]

$$k(s) = \left[\sum_{\mu}^{3K\text{-}L\text{-}1} B_{\mu,s}^2(s)\right]^{1/2} = \{k(s)^+ k(s)\}^{\frac{1}{2}}. \quad (8)$$

Because of this relationship, the $B_{\mu,s}(s)$ terms are called *curvature couplings*.

As will be discussed in the third part of this article, the coupling terms play an important role for the description of the mechanism of a chemical reaction: (1) They introduce changes in the vibrational modes along the reaction path. (2) They recover some of the anharmonicity, which is missing because of the harmonic potential. Both (1) and (2) are important prerequisites for the description of a chemical reaction, which involves bond-breaking and bond-forming processes and by that changes in the vibrational frequencies along *s*.

The nominator of the first term in the kinetic energy expression (5b) is the generalized momentum of the RP motion, and the denominator represents an effective mass μ_{eff}, which is of relevance for tunneling investigations. The direction of the mode vector $\mathbf{l}_\mu(s)$ at *s* is chosen in the way that the product $B_{\mu,s}(s)\, Q_\mu(s)$ becomes negative when $Q_\mu(s)$ is taken on the concave side of the RP. Hence, the curvature of the RP lowers the effective mass μ_{eff} and, accordingly, raises the tunneling probability.[15] If the sum in the denominator of the first term becomes smaller than -1 in the case of large curvature, $(\mu_{\text{eff}})1/2 < 0$ will indicate that the $(s, \{Q_\mu\})$ coordinate system of the RP is no longer suitable and that the concept of the RP has to be extended to a reaction surface being spanned by all those modes that are responsible for the large curvature couplings; see below.

EXTENSIONS OF THE ORIGINAL RPH

Reaction Path Coordinates Sets

Coordinate sets that describe a reacting system in the (3K-L)-dimensional configurational space by a 1D motion plus (3K-L-1) motions perpendicular to it have been generally termed *natural reaction coordinates*. Hofacker,[8] Marcus[9–11], Fischer and Ratner,[16] and Russeger and Brickman[17] used natural collision coordinates that define a RP as a curve where the classical local vibrational and internal centrifugal forces balance. Hougen et al.[13] developed a model for treating the large amplitude motions (LAM), which are

frequently observed in vibrational–rotational spectroscopy, apart from all the other internal coordinates. These ideas served as the framework for the generalized normal modes used by Handy et al. in their RPH. A number of different coordinate sets have been developed over the years to improve the performance of the RPH mostly with regard to dynamics studies, in particular tunneling and reaction rate calculations within the variational transition state theory (VTST) framework.[18] Some of these alternative RP coordinate sets belonging to the three major classes, *rectilinear*, *curvilinear*, and *action-angle* coordinate sets are discussed in the following. (Coordinates that can be expressed as linear combinations of Cartesians coordinates are conventionally called *rectilinear* and those that are nonlinear functions of Cartesians coordinates are called *curvilinear*.)

Cartesian Coordinates

Ruf and Miller[19] suggested a RPH in terms of Cartesian coordinates. Some Cartesian coordinates of the reaction complex are picked as 'system' (reaction coordinate), whereas the remaining Cartesian coordinates define the 'bath' (orthogonal reaction valley). The dependence of the potential on the bath coordinates is expressed as a Taylor expansion to second order. In this way, a linear coupling between system and bath results and a mass independent reaction path. They investigated the H-transfer in malonaldehyde using just one Cartesian coordinate as 'H-shift' parameter and received a less sharply curved reaction path, which led to better tunneling splitting than with the IRC path. However, the choice of system and bath coordinates is not free from arbitrariness and it is not obvious how to apply this strategy to larger reaction systems. The resulting path is no longer a minimum energy path (MEP) and as such not useful for mechanistic studies, as will be discussed in the section *the Unified Reaction Valley Approach and Reaction Mechanism*.

Curvilinear Internal Coordinates

The generalized normal-modes taken at nonstationary points along s are coordinate-dependent[20] and impact-calculated tunneling coefficients and rate constants. Curvilinear internal coordinates often outperform rectilinear coordinates in dynamics calculations based on the RPH and also remove the problem of imaginary frequencies emerging along the reaction path.[21–23] This shows that the appearance of one or more imaginary generalized normal mode frequencies along the path does not necessarily indicate a path bifurcation, it may simply reflect that the coordinates used are not appropriate for the reacting system in question. Redundant internal coordinates are the most widely used today and guarantee a smooth description of the reaction complex from the entrance to the exit channel where valence internal coordinates (bond lengths, bond angles, and torsions) are chemically the most evident.[21]

The curvilinear coordinates q_i can be expressed in terms of a power series of the Cartesian coordinate displacements

$$q_i = \sum_{j}^{3K} B_{ij}\left(R_i - R_i^0\right) + \frac{1}{2}\sum_{j,k}^{3K} C_{jk}^{i}\left(R_j - R_j^0\right)\left(R_k - R_k^0\right) + \cdots \quad (9)$$
$$i = 1, \ldots, F$$

with $F \geq (3K\text{-}L)$.

B_{ij} is an element of the Wilson **B** matrix[24]

$$B_{ij} = \left(\frac{\partial q_i}{\partial R_j}\right),$$

and C_{jk}^{i} is an element of the tensor $\mathbf{C}^i$ representing the quadratic term

$$C_{jk}^{i} = \left(\frac{\partial q_i}{\partial R_j \partial R_k}\right).$$

The gradient and Hessian of the curvilinear coordinates are related to their Cartesian counterparts by

$$\mathbf{g}^{\mathbf{q}} = \mathbf{A}^T\mathbf{g} \quad (10)$$

and

$$\mathbf{f}^{q} = \mathbf{A}^T\mathbf{f}\mathbf{A} - \sum_{i}^{F} g_i \mathbf{A}^T\mathbf{C}^i\mathbf{A} \quad (11)$$

with

$$\mathbf{A} = \mathbf{u}\mathbf{B}^T\mathbf{G}^{-1}, \quad (12)$$

where $\mathbf{u}$ is a diagonal matrix with the reciprocal atomic masses, $\mathbf{G}^{-1}$ is the generalized inverse of the Wilson **G** matrix,[24] which following the procedure of Pulay and Fogarasi[25] has a block structure eliminating the redundancies. Based on Equations (9)–(12), the generalized normal modes in terms of curvilinear internal coordinates along the reaction path can be derived by applying the formalism developed by Jackels et al.[23]

Nguyen et al.[22] found for the OH + H_2 → H_2O + H reaction that the use of standard rectilinear coordinates yields rate constant that are twice as large at 300 K as calculated with curvilinear coordinates. Along these lines, Natanson et al.[20] found that in the

case of $H + H_2$, $O + H_2$, and $CH_3 + H_2$, the vibrational frequencies evaluated with the original RPH led to a thinner adiabatic potential and, in this way, to an exaggeration of tunneling.

Quasirectilienar Vibrational Coordinates

Okuno et al.[26,27] suggested to use a RPH based on a quasirectilinear reaction path coordinate set constructed from a nonlinear combination of curvilinear internal coordinates. The name 'quasirectilinear' stems from the fact that these coordinates correspond to geodesic coordinates[28] in the reaction valley perpendicular to the RP. These coordinates are separated from rotations, and they are invariant under the transformation of the original internal coordinates. The authors conclude that because of these properties, improved reaction path dynamics should be obtained in the case of the zero-angular momentum assumption. Application of their RPH formulation to the $CH_4 + F$ reaction led to harmonic vibrational frequencies, which differ from those calculated with the original RPH of Handy et al.[4] and from those calculated with the curvilinear coordinates used to derive the quasirectilinear coordinates. The performance of this coordinate set with regard to rate constants and tunneling probabilities has not been reported yet.

Angle Action Coordinates and Vibrational Adiabaticity

To simplify the dynamics based on the RPH, one may assume that the motion along the reaction path is much slower than the motion perpendicular to the path. This vibrationally adiabatic assumption, which can be compared with the Born Oppenheimer separation of electronic and nuclear motion, leads to a description of a reactive process as 1D motion along the reaction path in an effective potential.

Pavlow-Verevkin and Lorquet[29] applied a RPH expressed in action angle coordinates to investigate exit-channel dynamics, (e.g., vibrational energy disposal into reaction products) in barrierless unimolecular reactions and to derive a measure for the validity of the vibrationally adiabatic assumption.[30] They could verify that regions of large reaction path curvature lead to a loss of vibrational adiabaticity, i.e., to a conversion between translational and vibrational energy, as described by the curvature-coupling coefficients $B_{\mu,s}(s)$.

For a system of two degrees of freedom (for an extension to 3K-L degrees of freedom, see Pavlow-Verevkin and Lorquet[29]) assuming zero angular momentum the action-angle RPH is given as[4]

$$H(s, p_s, q, J) = \frac{[p_s + J \sin q \cos q\, \omega'(s)/\omega(s)]^2}{2[1 + \sin q\sqrt{\sigma(s)}]^2} + V(s) + J\omega(s). \quad (13)$$

The vibrational motion perpendicular to the RP is described by the angle-action variables q and J. $\omega(s)$ corresponds to the s dependent harmonic frequency, and $\omega'(s)$ is the first derivative with respect to s.

The dimensionless-coupling parameter $\sigma(s)$ is defined as

$$\sigma(s) = 2J\,k(s)^2/\omega(s) \quad (14)$$

with the reaction path curvature $k(s)$.

The vibrationally adiabatic Hamiltonian for this system is given by averaging (13) over q (Ref 4)

$$H_{\text{as}}(s, p_s|J) = \left(\frac{1}{2\pi}\right)\int_0^{2\pi} H(s, p_s, q, J)\,\mathrm{d}q = \frac{p_s^2}{2[1-\sigma(s)]^{3/2}} + V_{\text{eff}}(s), \quad (15)$$

where the action J is a constant of motion. The effective potential is composed of $V(s) + J\omega(s)$ and a term depending on the internal energy of the system.[29] This leads to a dimensionless parameter

$$\mu(s) = [J\ \omega'(s)/\omega(s)]^2/[16\varepsilon(s)], \quad (16)$$

with the kinetic energy $\varepsilon(s)$. The term $\omega'(s)/\omega(s)$ is related to the diagonal of the Coriolis coupling matrix with element $B_{\mu,\mu}(s)$ being defined as[4]

$$B_{\mu,\mu}(s) = -\omega'_{\mu}(s)/2\omega_{\mu}(s), \quad (17)$$

where $B_{\mu,\mu}(s)$ describes how fast the vibrational frequency $\omega_{\mu}(s)$ changes along s.

Comparison of $H(s, p_s, q, J)$ and $H_{as}(s, p_s|J)$ leads to two independent conditions that must hold for vibrational adiabaticity, (1) $\sigma(s) \ll 1$ and (2) $\mu(s) \ll 1$.

(a) Holds when the amplitude of the vibration perpendicular to the path is smaller than the radius of the reaction path curvature; *dynamic coupling*.

(b) Holds when the change of the vibration perpendicular to the path is small, *static coupling*.[29]

The authors conclude that in a polyatomic molecule the reaction coordinate is preferentially coupled to vibrations with large σ and μ and that energy disposal into vibrational modes is preferentially

into soft modes characterized by large amplitudes (dynamic coupling) and a rapidly changing frequency along s (static coupling). Yan et al.[31] showed how the theoretical investigation of the energy flow between translations and vibrational modes along s can be combined with new experimental studies leading to a fruitful exchange between both disciplines.

Angle Action Coordinates for Nonzero Angular Momentum

Angle-action coordinates have also been used to derive a RPH that includes nonzero angular momentum **J** considering the rotational symmetry of a polyatomic reaction complex in 3D space and the conservation of total angular momentum. For this purpose, the three components of **J**, Jx, Jy, and Jz, must be expressed in terms of the canonical variables of rotation, e.g., by using the action-angle variables (J, qJ), (M, qM), (K, qK), where J is the magnitude of **J**, M and K are its projection onto space-fixed and body-fixed z-axes, and qJ, qM, and qK are their conjugated angle variables.[32] Since J and M are conserved quantities, the Hamiltonian does not depend on qJ and qM. The direction of the space-fixed axis is arbitrary and, therefore, the Hamiltonian is also independent of M. For a given value of **J**, the rotational part of the Hamiltonian can be written as[32]

$$\begin{aligned}\varepsilon_{\mathrm{rot}}^{\mathrm{J}}(K, q_k; s) = {} & A(s)\,(J^2 - K^2)\cos^2 q_k \\ & + B(s)\,(J^2 - K^2)\sin^2 q_k \\ & + C(s)\,K^2, \end{aligned} \tag{18}$$

where $A(s)$, $B(s)$, and $C(s)$ are the rotational constants for a given value of s.

New types of coupling terms have to be considered, which describe the coupling between rotation and the motion along the path and the coupling between rotations and vibrations. The latter is described (in first order) by the cross product of the eigenvectors of the transverse vibrational modes and by centrifugal distortion terms.[4]

Symmetry-Adapted Coordinates

Miller[33] showed that any geometrical symmetry of the reaction complex leads to selection rules in the dynamics of the reaction, e.g., leads to selection rules for the dynamical coupling between the reaction coordinate and the vibrational modes orthogonal to it. The use of symmetry-adapted coordinates leads to coupling coefficients between modes belonging to different irreducible representations that are identically zero. For example, Wardlaw[34] investigated the RPH using symmetry-adapted coordinates for the reactions CH_3 + X, where X = H, D. The coupling coefficients for CH_3, + H and CH_3, + D turned out to be the same in the transition state region and, therefore, could disprove the suggestion that an apparent isotope anomaly in the experimentally derived rates of these reactions might be caused from different dynamics along the reaction path.

Although useful for a symmetry-adapted transition state theory, the derivation of symmetry-adapted coordinates for a larger reaction system is a difficult task, and therefore its application is in so far limited.

Different Reaction Path Hamiltonian Models

Over the years, besides different RP coordinate sets different RPH models were developed. A selection will be discussed in the following.

Diabatic Reaction Path Hamiltonian

One modification of the original RPH concerns the harmonic reaction valley. Using a valley potential with appropriate anharmonic corrections, the potential energy part in the RPH adopts the form of Equation (19):[35,36]

$$\begin{aligned} V(s, \{Q_\mu\}) = {} & V_o(s) + \frac{1}{2!}\sum_\mu \omega_\mu^2(s)\, Q_\mu^2(s) \\ & + \frac{1}{3!}\sum_\mu\sum_\nu\sum_\lambda C_{\mu\nu\lambda}(s) Q_\mu(s) \\ & \times Q_\nu(s)\, Q_\lambda(s) \\ & + \frac{1}{4!}\sum_\mu\sum_\nu\sum_\lambda\sum_\sigma C_{\mu\nu\lambda\sigma}(s)\, Q_\mu(s) \\ & \times Q_\nu(s) Q_\lambda(s)\, Q_\sigma(s), \end{aligned} \tag{19}$$

where the coefficients of the cubic and the quartic terms are given by

$$C_{\mu\nu\lambda}(s) = \sum_i\sum_j\sum_k \frac{\partial^3 V(s)}{\partial x_i \partial x_j \partial x_k} l_{i,\mu}(s)\, l_{j,\nu}(s)\, l_{k,\lambda}(s) \tag{20}$$

and

$$\begin{aligned} C_{\mu\nu\lambda\sigma}(s) = {} & \sum_i\sum_j\sum_k\sum_l \frac{\partial^4 V(s)}{\partial x_i\, \partial x_j\, \partial x_k\, \partial x_l} \\ & \times l_{i,\mu}(s) l_{j,\nu}(s)\, l_{k,\lambda}(s)\, l_{l,\sigma}(s). \end{aligned} \tag{21}$$

The coefficients C cover (beside intramode anharmonic contributions) mode–mode coupling in the potential energy part of the RPH and, therefore, are called potential energy couplings. Contrary to the original RPH, frequencies $\omega_\mu(s)$ corresponding to modes of the same symmetry can now cross, i.e. they

undergo a local Fermi resonance in the crossing region. A RPH with a potential as defined in Equation (19) is therefore called a diabatic RPH.

A diabatic RPH may also be useful within the harmonic reaction valley approach if one considers a least motion path that interpolates linearly between two boundary points of a path region with strong curvature. Such a 'straight line' path is useful for tunneling descriptions in connection with H transfer reactions.[37] The kinetic part of the RPH for a straight-line path no longer contains curvature couplings since a straight line has zero curvature. The remaining Coriolis couplings in the kinetic energy can be transferred to the potential energy part by an appropriate transformation so that the kinetic energy part no longer contains any coupling terms, which is of advantage if one wants to quantize the RPH. The potential V along the straight-line path adopts the form shown in Equation (22)[37]

$$V(s,\{Q_\mu\}) = V_o(s) - \sum_\mu C_\mu(s)\, Q_\mu(s) + \frac{1}{2}\sum_\mu \sum_\nu Q_\mu(s)\Lambda_{\mu,\nu}(s)Q_\nu(s). \quad (22)$$

The linear term is a direct consequence of the fact that the straight-line path is no longer a MEP. The diagonal elements $\Lambda_{\mu,\mu}(s)$ can be interpreted as diabatic frequencies, which can cross independent of the symmetry of the corresponding normal modes. The off-diagonal elements $\Lambda_{\mu,\nu}(s)$ in the potential coupling terms describe transitions from mode μ to mode ν.

Quantum Mechanical RPH

Attempts have been made to replace the classical RPH by a (semi-)quantum mechanical RPH and to derive in this way a better description of the reaction dynamics. The kinetic energy part of the RPH can be quantized by replacing all momenta with the corresponding quantum mechanical operators. This is straightforward for a diabatic RPH based on the zero curvature ("straight-line") RP assumption for which all coupling terms are removed from the kinetic energy as described above. Also, the harmonic potential can be quantized as done by Billing,[38] who derived in this way a semiclassical RPH being useful for dynamics calculations. Another option is to treat the 3N-7 vibrational modes perpendicular to the RP with a second quantization approach as suggested by Billing.[39] This leads to a compact theory useful for estimating rate constants without having to construct the full PES. An overview of Billing's work in this field is given in Ref 40.

Gonzales et al.[41] recently introduced a quantum mechanical RPH describing the motion of a molecular system constrained to follow a RP embedded in the 3N-6 configuration space. Their ansatz is based on the Madelung–deBroglie–Bohm[42] interpretation of quantum mechanics. The constraint to motion along a predefined RP leads to a position-dependent mass term in the kinetic energy. Comparison against exact 3D quantum scattering calculations, in particular for the reaction F + H_2, shows the potential of this new method even for larger reaction systems.

Mixed Quantum-Classical RPH

Bladow et al.[43] introduced a mixed quantum-classical method based on the RPH for modeling the disposal of the exit-channel potential energy into the reaction products. In their model, Coriolis couplings are neglected, the transverse vibrations along the RP are treated quantum mechanically, whereas the motion along the RP is treated classically. Anharmonicity and deviation from the MEP are neglected as well. The analysis focuses on the reaction path curvature and the curvature couplings as they develop in the exit channel. Analysis of the four-centered decomposition reactions $C_2H_5X \rightarrow C_2H_4 + HX$, where X = F, Cl, reveals that in the case of Cl the elimination products are significantly more vibrationally excited, which the authors relate to a later reaction path curvature for the HCl elimination path.

Unified Semiclassical Perturbation and Infinite Order Sudden Approximation and Path Integrals

Miller and Shi[44] combined two approximate dynamics models, the semiclassical perturbation theory and the infinite order sudden approximation and incorporated the unified models into the original RPH. They derived in this way a reasonable, semiquantitative description of the molecular collision processes, even for polyatomic systems.

Miller et al.[45] showed that Boltzmann rate constants could be obtained by evaluating the path integral of a reactive flux correlation function, avoiding in this way first to calculate the complete state-to-state reactive scattering problem and then to Boltzmann average the results. Yamashita and Miller[46] incorporated the path integral idea into the framework of the RPH model for a general polyatomic reaction. In this way, the correlation function, the time integral of which is the rate constant, can be expressed as single path integral over only one degree of freedom (the reaction coordinate). Effects of tunneling, 'frictional'

effects on the reaction coordinate due to coupling to other degrees of freedom, and the effects of recrossing the transition state dividing surface are all correctly accounted for in their approach. Numerical tests of the formulas for the 3D version of the H + H_2 reaction showed excellent agreement with the (known) accurate results for this system. For an overview on this topic, see Ref 47.

Solution Reaction Path Hamiltonian

Lee and Hynes[48,49] developed a solvent reaction path Hamiltonian (SRPH) for the description of chemical reactions in polar solvents. The solvent is treated as a polarizable continuum characterized by its dielectric constant. The progress of the reaction from reactants to products is described by a single coordinate X_{Re} (ignoring any other internal molecular modes), which is chosen on the basis of chemical intuition, e.g., in the case of the ionic dissociation AB $\rightarrow$ A^+ + B^- the reaction coordinate X_{Re} is simply the distance between atoms A and B. In analogy to the original RPH, the coordinate X_{Re} is associated with the LAM along the RP whereas the orthogonal motions are represented by a coordinate X_{Sol} covering all solvent rearrangements. Solvent polarization and, by this, the free enthalpy $G_{eq}(X_{Re})$ of the reaction complex in the solvent is calculated for each point along the RP utilizing a X_{Re}-dependent charge distribution function. In this way, the potential energy part of the RPH adopts the form of the free enthalpy function $G(X_{Re}, X_{Sol})$:

$$G(X_{Re}, X_{Sol}) = G_{eq}(X_{Re}) + \frac{1}{2} K_{Sol}(X_{Re})[\Delta X_{Sol}(X_{Re})]^2. \quad (23)$$

The first term is the equilibrium free enthalpy, i.e., the solvent polarization has adjusted to the charge distribution of the reaction complex at point X_{Re}, and the second term gives the free enthalpy part due to deviation from equilibrium polarization at X_{Re}. $K(X_{Re})$ is a X_{Re}-dependent solvent force constant.

Truhlar et al.[50] generalized the Lee–Hynes SRPH model by defining the solute atomic charges as a function of solute geometry. Chuang and Truhlar[51] constructed a more general SRPH model including the nonequilibrium solvation effect by means of a general linear response method. Ohmiya and Kato[52] introduced a SRPH, which combines the reference interaction site model (RISM) integral equation theory[53] for molecular solvents with a quantum mechanical description of the solute named *ab initio* RISM-SCF. In this way, the molecular aspects of solvents are included and local solute–solvent interactions such as hydrogen bonding can be described.

Hu et al.[54] performed a RPH analysis for a Claisen and a Diels–Alder reaction in solution simulating the solvent by two explicit water molecules. This approach, although simple, provides useful qualitative information about dynamical solvent effects, which can be in particular in the case of comparative studies.

RPH for Enzyme Reactions

Lu and Yang[55] used the original RPH ideas to develop a *reaction path potential* for statistical mechanics and dynamics simulation of chemical reactions in enzymes and other complex systems. They derived the reaction path potential as an analytical energy expression of the combined quantum mechanical (QM) and molecular mechanical potential (MM) energy along the MEP. An expansion around the MEP was made in both the nuclear and the electronic degrees of freedom for the QM subsystem internal energy, whereas the energy of the subsystem described with MM remained unchanged. The QM charges were treated as polarizable in response to the changes in both the MM and the QM degrees of freedom. The feasibility of the reaction path potential and its application to reaction free energy calculations was illustrated studying of a proton transfer reaction catalyzed by the enzyme triosephosphate isomerase.

For a recent application of the reaction path potential to enhance the efficiency of the *ab initio* QM/MM minimum free energy path calculations, see Ref 56.

Reaction Surface

In the case of "heavy—light–heavy" atom transfer reaction (e.g., I + HI $\rightarrow$ IH + I), the RP is sharply curved.[57] Similar observations can be made for other H transfer reactions. In these cases, the basic assumption of the original RPH, namely that the (3K-L)-dimensional coordinate space can be spanned by one large amplitude motion being connected with the displacements s along the RP and 3K-L-1 small amplitude motions (SAM) being associated with the normal coordinates $Q\mu$ orthogonal to the RP, breaks down. One has to treat all LAMs (the 'system') separately from the SAMs (the 'bath') in the RPH to obtain a reasonable description of the reaction dynamics, e.g., tunneling coefficients and rate constants. Carrington and Miller[58] derived a RPH for a reaction surface, e.g., the case of two large amplitude motions, which they successfully applied to the description of intramolecular hydrogen transfer in malonaldehyde.[59] Miller and Schwartz[60] used the 'system-bath' decomposition of the RPH model to

derive a model for polyatomic scattering. Only those few transverse modes that couple strongly with the RP define the system in which the dynamics are treated accurately, whereas the coupling to the remaining transverse modes ('bath') is treated by first-order perturbation theory.

Tew et al.[62] applied their MULTIMODE-RPH method (Multimode is a variational scheme for the calculation of ro-vibrational energy levels of polyatomic molecules) to a reaction surface study of malonaldehyde. They achieved an accurate description of the tunneling transfer and in addition, insight into the nature of the OH-stretching vibrations. The surface study suggests that the ν_1 fundamental frequency is much lower than previously estimated due to the substantial transition state character.

Nauts and Chapuisat[35] proposed to partition the 3K-L internal coordinates of the reaction complex into n internal coordinates R_k^S, which provide a description of the LAMs, and 3K-L-*n* normal coordinates Q_μ, describing the SAMs. The coordinates R_k^S span an *n*-dimensional *reaction surface*, which is orthogonal to the remaining (3K-L-*n*)-dimensional subspace of the SAMs. For a minimum energy surface, zero angular momentum, and harmonic energy walls, the reaction surface Hamiltonian takes the form of Equation (24)[35]:

$$H\left[\left\{R_k^S\right\},\{P_k\},\{Q_\mu\},\{P_\mu\}\right] = \frac{1}{2}(\mathbf{P}_R^+,\mathbf{P}_Q^+)\begin{pmatrix}\mathbf{G}_{RR} & \mathbf{G}_{RQ}\\ \mathbf{G}_{QR} & \mathbf{G}_{QQ}\end{pmatrix}\begin{pmatrix}\mathbf{P}_R\\ \mathbf{P}_Q\end{pmatrix} + V_o(\mathbf{R}^S) + \frac{1}{2}\sum_\mu \omega_\mu^2(\mathbf{R}^S)Q_\mu^2(\mathbf{R}^S), \quad (24)$$

where the matrix **G** (related to the Wilson **G** matrix) is partitioned into elements G_{RR}, G_{QQ}, etc. according to a partitioning of the total space into the space of the surface coordinates $\{R_k^S\}$ and the space of the normal mode coordinates $\{Q_m\}$. Couplings between on- and off-surface modes are covered by the elements of the $\mathbf{G}_{QR}$ submatrix.

The choice of the coordinates $\{R_k^S\}$ is not trivial and requires chemical intuition. Frequencies, normal modes, and coupling coefficients are complicated functions of $\mathbf{R}^S$, so that the simplicity of the original RPH of Handy et al. is no longer given.

Curvature-Based Reaction Path

Taketsugu and Gordon[63] introduced a 'dynamic' RPH based on the reaction coordinate *s* and a curvature coordinate ρ that should be effective when the RP is sharply curved and the original adiabatic RPH becomes inappropriate. In this way, path tangent and curvature vectors span a reaction plane. The curvature coordinate ρ defines displacements along the curvature vector $\mathbf{k}(s)$ and, accordingly, describes any coupling between the translational motion along the RP and a transverse vibrational motion that causes a large curvature vector. Couplings with the remaining 3K-L-2 normal modes $\mathbf{l}_\mu$ do not play any role and can be ignored. The corresponding RPH has the following form:

$$H[s,p_s,\rho,p_\rho,\{Q_\mu\},\{P_\mu\}] = \frac{1}{2}\frac{p_s^2}{[1+\rho\,k(s)]^2} + V(s) + \frac{1}{2}p_\rho^2 + \frac{1}{2}\omega_\rho^2(s)\rho^2 + \sum\left[\frac{1}{2}P_\mu^2 + \frac{1}{2}\omega_\mu^2(s)Q_\mu^2(s) - k_{\mu,\rho}(s)Q_\mu(s)\right], \quad (25)$$

where p_ρ is the conjugated momentum of ρ, $k_{\mu,\rho}(s) = \partial V^2(s)/\partial Q_\mu \partial_\rho$ is an off-diagonal element of the force constant matrix, which describes a potential energy coupling between ρ and Q_μ. Coriolis coupling terms of the 3K-L-2 normal modes are neglected. Kinetic energy coupling between *s* and ρ is described by the term $\rho\,k(s)$, whereas couplings between *s* and Q_μ are covered by the curvature $k(s)$. Monitoring of the changes in the reaction plane along *s* leads to a dissection of a chemical reaction into distinct phases as done for dissociation of thioformaldehyde.[64]

Reaction Volume and Generalized Reaction Valley

Colletti and Billing[65] presented a numerical scheme that goes beyond a reaction surface, e.g., it allows for three large amplitude motions and in this way leads to a reaction volume. The authors discuss practical application of this concept for determining state resolved cross sections or rates. Walet et al.[66] suggested a generalized reaction valley approximation decoupling one or a few low-frequency modes from the remaining higher frequency modes of a polyatomic reaction system. In this way, they derived multidimensional subspaces that are optimally decoupled. Their approach differs from the original RPH in the way that there are couplings in both kinetic and potential energy terms.

Reduced Dimension RPH

Jang and Rice[67] derived a two-dimensional RPH to generate an accurate description of the dynamics of unimolecular isomerization reactions. The basic idea of their approach is to derive a two-dimensional (2D) RPH based on two isomerization coordinates. The subsequent dynamics of the system is then reduced

to two degrees of freedom although each of these degrees of freedom has an implicit dependence on all other degrees of freedom of the molecule.

A RPH for Time-Dependent SCF Dynamics

Fang and Schiffer-Hammes combined the time-dependent self-consistent-field (TDSCF) method with the RPH.[68] They derived the equations of motion for the TDSCF-RPH dynamics for three different cases, (1) all curvature and Coriolis couplings are zero, (2) zero reaction path curvature but nonzero Coriolis couplings, (3) small reaction path curvature and zero Coriolis couplings. In a subsequent paper, Fang and Hammes-Schiffer[69] showed that for these three cases the dynamics are reducible to a 1D numerical time propagation of the reaction coordinate. They also discussed how the TDSCF approach could be combined with a diabatic RPH in case of large reaction path curvature.[70] To cover a broader range of reactions, the authors suggest an extension to a multiconfiugration TDSCF-RPH methodology.

RHP and Tunneling

Within the framework of VTST, it has been shown that the curvature of the RP and, hence, the coupling terms strongly influence quantum mechanical tunneling through the barrier.[18] The larger the coupling terms, the more facile tunneling is. Tunneling models of increasing sophistication based on the RPH have been suggested and have been applied within the framework of VTST. For a recent review of this topic, see Ref 71 and references therein. Recently, this approach has been applied even to a larger biological system applying ensemble averaged VTST.[72,73]

Fehrensen et al.[74] suggested a simplified formulation of the harmonic RPH to calculate mode-specific tunneling splitting and stereomutation times, which in contrast to other reduced dimensionality models (see, e.g., Ref 70) includes all vibrational degrees of freedom, even for larger systems. As an example, they presented a complete *ab initio* description of the multidimensional torsional tunneling dynamics in methanol. Wang and Bowman[75] developed a simplified tunneling model being based of a RPH in the zero-curvature approximation coupled with a 1D Hamiltonian in the imaginary-frequency rectilinear normal mode of the saddle point. Tunneling splitting results for H and D-transfer in malonaldehyde and for D + H_2 in three dimensions were encouraging.

Luckhaus[76] proposed a 2D RPH model for the description of large curvature tunneling, which is typical for H exchange. He derived a nonorthogonal representation of the RPH in terms of local harmonic oscillators distributed along the RP. His model turned out to be robust with regard to variations in the RP and bifurcation and seems to be promising also for larger systems.

RPH Liouville Approach for Rate Constants

Gonzales et al.[77] derived a 2D RPH in phase space, collecting the influence of all molecular degrees of freedom. This reduction of dimensionality permits the solution of the classical Liouville equation for the evaluation of the flux required in a rate constant evaluation. The authors showed that the rates obtained by this procedure are a new rigorous upper bound to the exact classical rate constant, which in turn is lower than (or at most equal to) a transition state theory (TST) rate. A revised form based of this reaction path Liouville (RPL) method (being based on the time-dependent first integral method of the theory of differential equations)[78] leads in addition to rate constants also to the kinetic energy storage in the normal modes as function of time. The only ingredients needed are gradients, Hessians along the reaction path plus the mathematical solution of a 3D differential equation. This makes the method attractive for rate constant calculations of polyatomic systems. The normal mode kinetic energy (NMKE) analysis provides complementary information to the geometrical changes of the reaction complex or the changes of its vibrational frequencies along the reaction path. The authors applied their new method to an SN_2 reaction, a H-transfer reaction, and an addition reaction to unsaturated hydrocarbons. They could confirm in all cases that the RPL rate constant is smaller than the TST rate constant.

Generalized RPHs for Rate Constants for Polyatomic Molecules

Gonzales et al.[79,80] reformulated the classical RPH of Handy et al. using a linear expansion of the gradient in internal coordinates. Both, kinetic and potential energy are expressed as function of s, the gradient and the Hessian along s. They derived an explicit relationship between the arc length s and the internal coordinate set and a Bernoulli-type dynamical equation for s describing the time dependence. This leads to a computationally efficient direct dynamics method. In addition, they generalized the original RPH to a form that it becomes independent of the specific choice of a reference path.[81,82] The necessary and sufficient requirement is that the reference path, defined in terms of its dependence on a freely chosen parameter, must not explicitly depend on this parameter. One possible reference path tested by the authors is a Newton path.[83] The Newton path properly describes bifurcation points and leads to a reliable description of

rearrangement processes. Although the Newton path turns out to be 'wigglier' than the IRC, it leads to comparable rate constants. The authors concluded that for a rate constant calculation any reference path fulfilling the necessary and sufficient condition is suitable as long as it is a good average path for the computation of the distribution function along it.

THE UNIFIED REACTION VALLEY APPROACH AND REACTION MECHANISM

The main focus in connection with the RPH was and still is to use it as a tool for the calculation of the dynamics of a chemical reaction, in particular the calculation of rate constants and tunneling coefficients. There are mechanistically oriented studies focusing on mode-specific enhancement of reaction rates via the analysis of the normal mode coupling coefficients, $B_{\mu,s}(s)$ or the energy dissipation via the analysis of the normal mode Coriolis coupling coefficients $B_{\mu,\nu}(s)$ like the work of Pewlov-Verkin and Lorquet,[29] the work of Bladow et al. or the NMKE analysis of Gonzales et al.,[77] discussed in this article. Other examples can be found in Refs 84–87. These investigations are a valuable resource for laser spectroscopists working in the field of vibrationally driven reactions,[88] which includes both enhancement of reaction rates, manipulation of energy disposal, and promotion of a certain product channel by mode selective excitation. However, the depth of mechanistic information provided by the RPH has not fully been exploited in a systematic way. An exception so far is the work based on the unified reaction valley approach (URVA), which will be discussed in the following[7,89,90]: URVA determines the energy profile $E(s)$, the reaction force $F(s)$ as well as higher derivatives of $E(s)$, geometrical parameters $q(s)$ and their derivatives, the internal forces and vibrational modes of the reaction complex, the RP direction $\mathbf{t}(s)$ and curvature $\mathbf{k}(s)$, coupling and Coriolis coupling coefficients at each point s along the RP, where the reaction path curvature plays a key role. URVA is based on the original RPH of Handy et al., a special ordering of the normal modes along the reaction path,[91] and the use of adiabatic localized normal modes, which are introduced below.

Central Role of the Reaction Path Curvature

A chemical reaction can be described as the consequence of the favorable interaction of two events, a molecular collision at an angle that enables energy transfer and a vibrational excitation that leads to bond loosening and cleavage. Chemical reactions start with a vibrational motion that is forced to adopt larger and larger vibrational amplitudes until bond cleavage occurs. Therefore, a chemical reaction requires that at least one bond stretching motion vanishes and/or a new one appears.[89,92] This implies a curving of the reaction path. An exclusively straight reaction path with zero curvature indicates a physical rather than chemical process. All vibrational motions of the reaction complex in a physical system are conserved, and consequently both Coriolis and curvature couplings are zero. Hence, exploration of the scalar reaction path curvature (as defined in Eq. (7)) along s detects the locations on the reaction path where the chemical changes of the reaction complex take place. The curving of the path is a measure of the energy change connected with the chemical processes. Each chemical event (like bond breakage or bond formation corresponds to a local curvature maximum flanked by two curvature minima, e.g., locations with minimal change of the reaction complex.

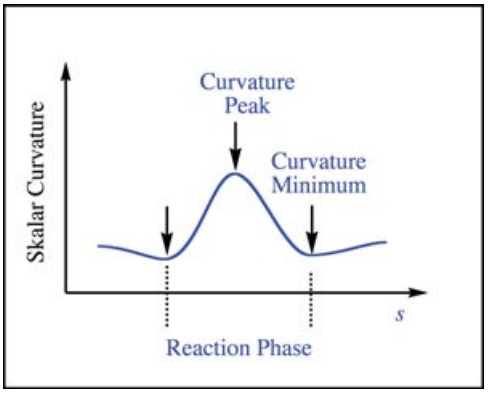

FIGURE 1 | Definition of a reaction phase based on the scalar curvature $k(s)$ plotted along the reaction paths. A reaction phase is defined by a curvature peak and the reaction path range given by the flanking curvature minima.

Therefore, Cremer and Kraka[89,92] define a reaction phase as the reaction path region from one curvature minimum to the next, characterized by a curvature maximum (see Figure 1). Different chemical reactions possess different curvature patterns with a different number of reaction phases, which can be used as their *fingerprints* as discussed below.

Adiabatic Internal Coordinate Modes

Further insight into the mechanism can be obtained by a decomposition of the reaction path curvature into curvature-coupling coefficients. In the original RPH of MHA, the decomposition is done in terms of

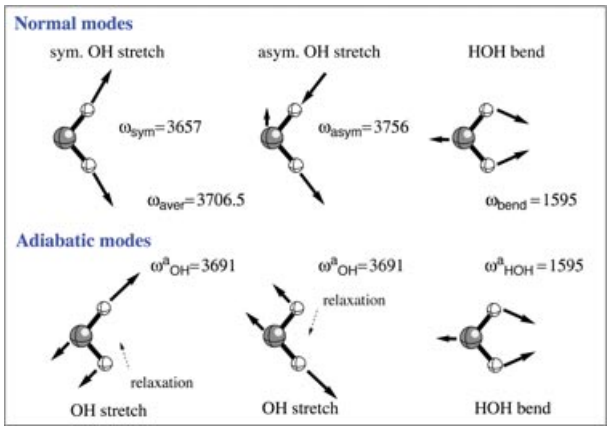

FIGURE 2 | Schematic representation of the three normal modes of the water molecule (from left to right): symmetric OH stretching, asymmetric OH stretching, and HOH bending mode (top); adiabatic OH stretching and HOH bending modes (bottom). Displacement arrows are given not to length scale to illustrate atom movements. Dashed arrows indicate movement of H atoms due to adiabatic relaxation.

generalized normal modes. However, normal modes are delocalized.

Therefore, to determine which internal coordinate, e.g., which bond length, bond angle, or torsion drives the reaction at what point on the reaction path, a decomposition into local internal vibrational modes being associated with the geometrical parameters used to describe the reaction complex is necessary. This is possible with the adiabatic internal coordinate modes (AICoMs) first introduced by Konkoli et al.[93–96] and Cremer and coworkers.[97] Each AICoM of a molecule is associated with just one internal coordinate q_n independent on all other internal coordinates q_m ($m \neq n$). Only atoms of the structural unit being described by q_n vibrate, whereas the rest of the molecule is allowed to relax so that the potential energy adopts a minimum. This is called an adiabatic motion. (Figure 2 compares a delocalized normal mode with its adiabatic localized counterparts for the water molecule.) The mathematical derivation of AICoMs is described in the *Appendix*.

AICoMs can be defined for equilibrium points on the PES as well as for all points along the RP where in the latter case it is required that the harmonic part of the potential energy in Equation (5a) is minimized with regard to displacements in the (3K-L-1)-dimensional vibrational space whereas relaxing all internal parameters but one. In this way, generalized adiabatic modes $\mathbf{a}_n(s)$ together with the corresponding adiabatic frequencies $\omega_n(s)$ and force constants $k_n(s)$ are obtained.

With the help of the generalized adiabatic modes $\mathbf{a}_n(s)$, both normal modes $\mathbf{l}_\mu(s)$, the reaction path direction $\mathbf{t}(s)$ and curvature vector $\mathbf{k}(s)$ can be analyzed utilizing appropriately defined amplitudes $A_{n,m}(\mathbf{l};s)$, $A_{n,s}(\mathbf{t};s)$, and $A_{n,s}(\mathbf{k};s)$[93–96]

$$A_{k,\mu}(\mathbf{l},s) = \frac{[\mathbf{l}_\mu^+(s)\,\mathbf{F}(s)\,\mathbf{a}_k(s)]^2}{[a_k^+(s)\,\mathbf{F}(s)\,\mathbf{a}_k(s)]\;[\mathbf{l}_\mu^+(s)\,\mathbf{F}(s)\,l_\mu(s)]} \tag{26}$$

$$A_{k,s}(\mathbf{t},s) = \frac{[g^+(s)\mathbf{M}^{-1}(s)\mathbf{b}_k(s)]^2}{[g^+(s)\,\mathbf{M}^{-1}(s)\,\mathbf{g}(s)]\,[\mathbf{b}_k^+(s)\,\mathbf{M}^{-1}(s)\,\mathbf{b}_k(s)]} \tag{27}$$

$$A_{k,s}(\mathbf{k},s) = \frac{[\mathbf{k}^+(s)\,\mathbf{M}(s)\,\mathbf{a}_k(s)]}{[a_k^+(s)\,\mathbf{M}(s)\,\mathbf{a}_k(s)]^{1/2}}, \tag{28}$$

which decompose generalized normal modes $\mathbf{l}\mu(s)$, (Eq. (26)), the reaction path direction $\mathbf{t}(s)$ (Eq. (27)), and the curvature vector $\mathbf{k}(s)$ (Eq. (28)) in terms of generalized adiabatic modes associated with internal coordinates used in the description of the reaction complex. The metric $\mathbf{F}$ guarantees a dynamical characterization of normal modes, whereas the metric $\mathbf{M}$ provides a kinetic characterization.[93–96] Amplitude $A_{k,s}(\mathbf{k},s)$ has the same dimension as $B_{\mu,s}(s)$, and, for $\mathbf{l}_\mu = \mathbf{a}_k$, amplitude $A_{k,s}(\mathbf{k},s)$ and coefficient $B_{\mu,s}(s)$ are equal. $\mathbf{g}(s)$ is the gradient vector at s.

Representative Reaction Path for Reactions with a Barrier

Different reaction paths can be chosen when investigating the reaction dynamics because they are used in connection with the statistical averaging of trajectories for the calculation of reaction rates as discussed by Gonzales et al.[82] However, in the case of a mechanistic study within the URVA framework one has to follow the most energy-efficient pathway of the reaction complex. Therefore, one has to choose a representative path, which stays close to the MEP, which for an elementary reaction with a transition state can be considered as the floor line of the reaction valley.[100] Usually the IRC path tends to follow the valley floor line, especially in the convex part of the PES between minimum and inflection point about halfway up to the transition state.[100] It has been pointed out that in the concave region between inflection point and transition state, the IRC path may deviate from the valley floor line.[100] However, small deviations from the floor line are of little consequence for the mechanistic discussion and, therefore, the IRC path is the path of choice for reactions with a barrier.

Representative Reaction Path for Reactions Without a Barrier

An IRC path does not exist for chemical reactions without a barrier. In this case, Newton trajectories[101]

turn out to be a useful tool for deriving a representative path. Newton trajectories are defined by the condition that a preselected gradient direction is kept by all points on the path, which can be considered as a generalization of the distinguished reaction coordinate approach.[102] Since any gradient direction can be chosen, Newton trajectories do not lead to a unique path. Instead, a family of Newton trajectory curves connects stationary points with a difference of order 1, for example minimum and transition state.[101] Quapp et al.[103] showed that in the case of a barrierless reaction Newton trajectories bundle in the exit channel of the reaction valley before merging onto the energy plateau. This makes it possible to determine a central point in the valley from where a representative downhill path can be started. There is also the possibility that the reaction valley opens up to a broad bowl as in the case of a cirque created by a glacier. In this case, the Newton trajectories can be used to describe seize and boundaries of the cirque, which again makes it possible to find a suitable starting point for a representative down hill path. The latter situation was encountered for the chelotropic addition of methylene to ethene yielding cyclopropane.[103,104]

Strategy of an URVA Analysis

The analysis of the reaction mechanism based on URVA utilizes the close relationship between reaction complex and reaction path to overcome dimensionality problems and the problem of quantitatively identifying, among the multitude of geometrical parameters, the few that drive important structural or electronic changes of the reaction complex.[89,92] The analysis of the 3K-L geometry parameters $q(s)$ along s and the identification of those changes in $q(s)$, which are relevant for the reaction mechanism, becomes tedious and ambiguous, in particular for larger reaction systems.

URVA solves these problems by a shift in the analysis from the reaction complex to the reaction path. The changes in the geometry of the reaction complex during the reaction are embedded in the reaction path, which is also defined in (3K-L)-dimensional space and on first sight does not seem to offer any advantages for the mechanistic analysis. However, the reaction path can be considered as a smooth, curved line, which is fully characterized by just three rather than (3K-L) quantities at each path point s. These are the path direction given by the tangent vector $\mathbf{t}(s)$, the path curvature $\mathbf{k}(s)$, in particular the scalar curvature $k(s)$, and the path torsion given by $\tau(s)$. The latter parameter is of little relevance because helical or loop-type paths have not been observed. Hence, it is sufficient to analyze just path direction and path curvature as a function of s.

URVA decomposes the translational motion in path direction and the vibrational motions orthogonal to the path direction into AICoMs driven by internal coordinates that are used to describe the reaction complex. Accordingly, if there is an internal coordinate q that dominates the path direction it will provide only a small or no contribution to the transverse vibrational modes of the reaction complex and vice versa. Therefore, there are two ways of analyzing the reaction mechanism: (1) via the path direction and (2) via the path curvature. Since the latter is much more sensitive and physically related to the changes in the adiabatic force constants (i.e., the first derivative of $k_a(s)$ with regard to s),[92] which in turn measures the polarizability of a bond, URVA is primarily based on the analysis of the path curvature and uses the path direction only to obtain complementary information. By analyzing the curvature in terms of adiabatic curvature coupling coefficients, a connection to the changes in the geometry of the reaction complex is made because the internal coordinates $q(s)$ that drive the adiabatic modes with large curvature coupling coefficients determine in this way also the curvature. Normal mode curvature and Coriolis-coupling coefficient are used to determine energy transfer and energy dissipation, as discussed above, whereas adiabatic curvature-coupling coefficients provide the basis to elucidate the reaction mechanism.

Hence the key feature of the URVA analysis is to first plot the scalar reaction path curvature $k(s)$ as a function of s, next to determine the maxima and minima of $k(s)$ leading to the different reaction phases of the chemical reaction. Decomposition of $k(s)$ into AICoMs will lead to a characterization of the reaction phases, e.g., by determining which internal parameters are driving the reaction. Next, geometry and other molecular properties will be investigated at the curvature maxima (center points of chemical change) and minima (points of least chemical change). Hence instead of investigating the reaction complex in (3K-L)-dimensional space, the focus is just on a few internal parameters, dominating the reaction, as outlined in Figure 3.

Curvature Patterns for Different Reaction Families

Use of URVA in mechanistic studies has led to an advanced understanding of chemical reactions,[7,89,90,92,103–108] which will be discussed in the following for selected chemical reactions of different type. The discussion will be limited to the

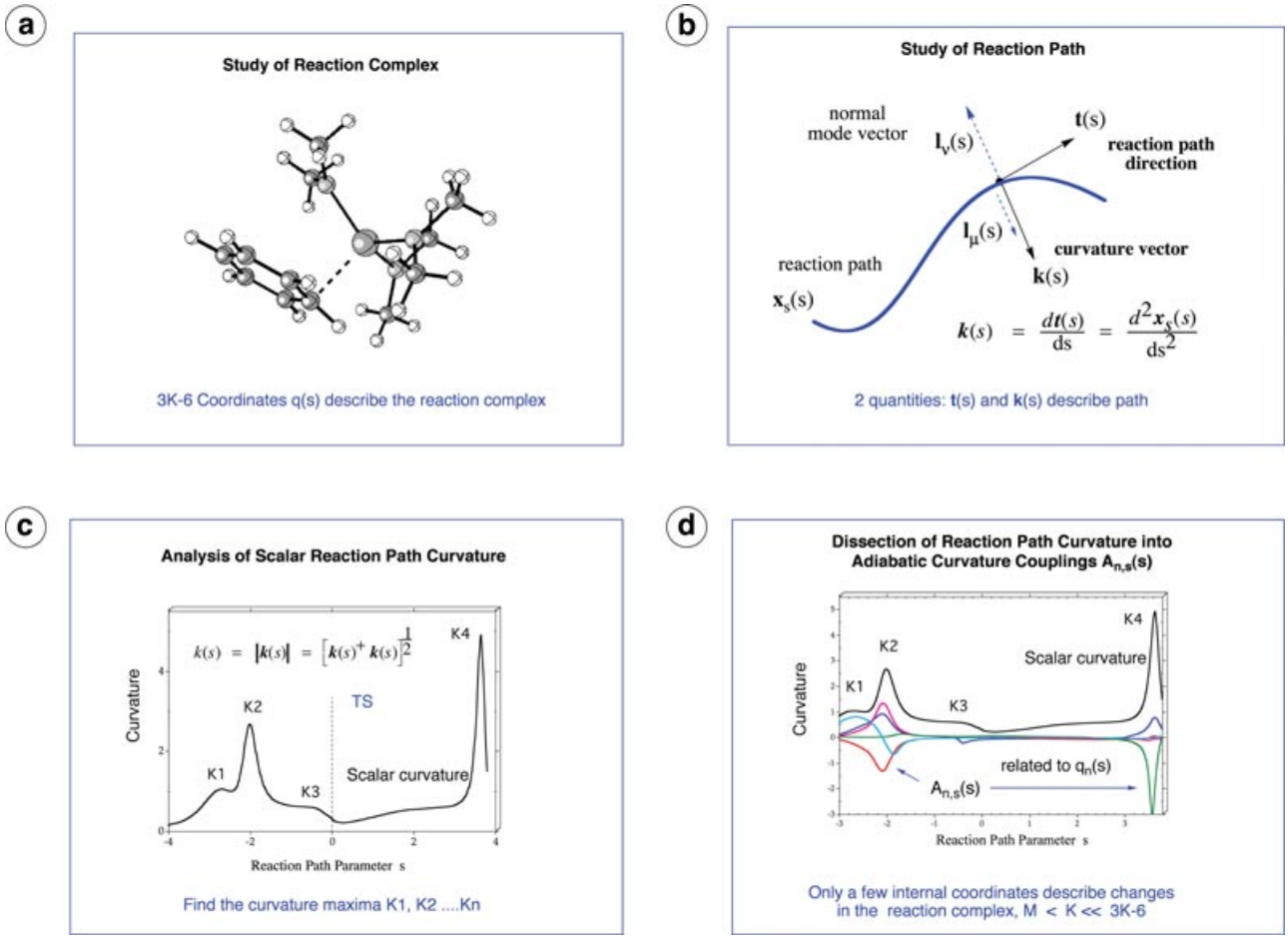

FIGURE 3 | Strategy of an URVA analysis. (a) Study of the reaction complex requires the analysis of 3K-6 internal coordinates $q_n(s)$. (b) The same information is contained in the direction $\mathbf{t}(s)$ and the curvature $\mathbf{k}(s)$ of the reaction path. Normal modes $\mathbf{l}_\mu(s)$ or $\mathbf{l}_\nu(s)$ can couple with curvature $\mathbf{k}(s)$ if properly aligned. (c) To obtain this information, the scalar curvature $k(s)$ is calculated. (d) Dissected into adiabatic curvature couplings $A_{n,s}(s)$, which identify all important changes of the internal coordinates $q_n(s)$ of the reaction complex. Just few ($M < K$) rather than 3K-6 internal coordinates have to be analyzed to describe structural changes of the reaction complex.

scalar curvature pattern, e.g., the reaction phases and curvature decomposition into AICoMs leading to the *fingerprints* of a reaction. For a detailed URVA analysis, the reader should refer to.—Refs 89, 90, 92, 103–109.

Hydrogen Exchange Reactions

In Figure 4, the scalar reaction path curvature $k(s)$ and its decomposition into adiabatic coupling coefficients $A_{n,s}(s)$ is shown for the hydrogen exchange reaction $CH_3 + H_2 \rightarrow CH_4 + H$.

The curvature diagram shows three curvature maxima defining four different reaction phases. In phase 1, the van der Waals region, pyramidalization of the methyl radical takes place; phases 2 and 3 are characterized by breakage of the HH bond and formation of the new CH bond, whereas phase 4 describes the product adjustments. We find that the HH-stretching motion is associated with K2 and the CH-stretching motion with K3. However the CH mode contributes also to K2 and the HH mode to K3 as can be seen here by the negative R2 and R1 components. (A negative $A_{n,s}(s)$ value means that the corresponding internal coordinate motion resists a curving of the path and the electronic structure changes associated with it.) First there is exchange repulsion between C and H and after the transition state (TS) exchange repulsion drives the H atoms apart. We learn from such a decomposition that HH bond rupture and CH bond formation start at the same time and terminate at the same time, only with different weights, first HH cleavage dominates then the CH bond formation. The unpaired electron in the sp^3-hybrid orbital of the methyl radical extends more into space than the s-electron of the H atom. Accordingly, the far-range polarizing power of the methyl radical is

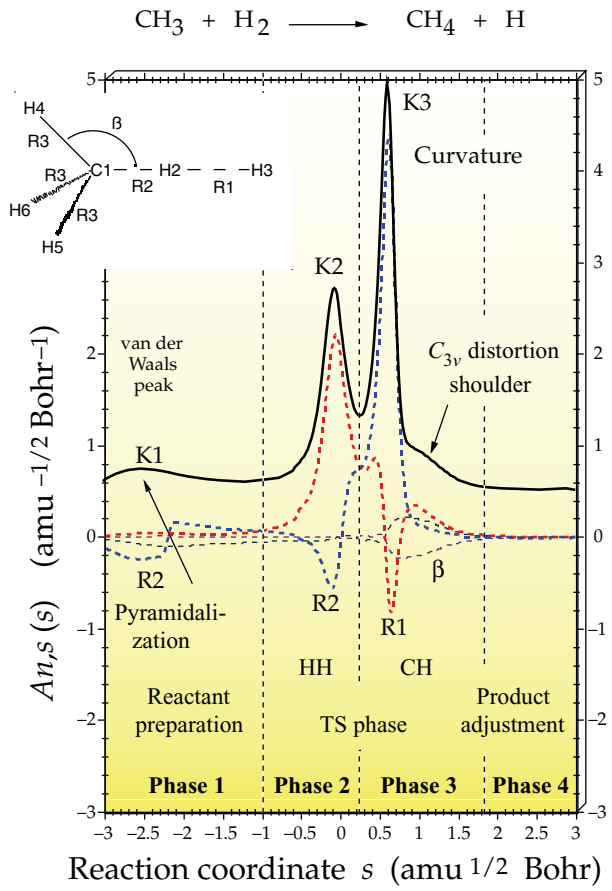

FIGURE 4 | Decomposition of the scalar reaction path curvature $k(s)$ (bold black line) of $CH_3 + H_2$ reaction terms of adiabatic curvature coupling coefficients $A_{n,s}(s)$ (colored lines). The curvature $k(s)$ has been shifted by 0.5 units to more positive values to facilitate the distinction between $k(s)$ and $A_{n,s}(s)$. K1–K4 denote the curvature peaks. Vertical lines separate the reaction phases. The position of the transition state corresponds to $s = 0$ amu$^{\frac{1}{2}}$ Bohr. UMP2/6-31G(d,p) calculations.[90]

larger than that of H. Despite the fact that the HH bond is stronger than the CH bond in CH_4, curvature peak K2 (associated with the HH bond) is broader and smaller than K3 (associated with the CH bond, Figure 4) because under the polarizing power of the methyl radical the HH bond starts earlier to deform and polarizes smoother. If a C–H bond in CH_4 is attacked by an H atom (back reaction), deformation of methane begins at close range, which is reflected in the curvature diagram of Figure 4 by a shoulder preceding the CH-cleavage peak K3. We have recently shown[92] that the curvature is related to the change in the vibrational frequencies rather than their magnitude or the difference of the magnitudes. Frequency ω(HH) decreases slower than ω(CH) increases, and this can be directly related to the fact that curvature peak K2 associated with the breaking of the HH bond is smaller and broader than the curvature peak K3 associated with the formation of the CH bond. Since the force constant is directly related to the frequency, we suggest to use AICoM-stretching force constants of cleaving bond AB, k_a(AB)(s) and forming bond BC, k_a(BC)(s) to describe the path curvature. Work is in progress to derive a relationship between the scalar curvature and the sum of the first derivatives, k'(AB)(s) + k′(BC)(s).

Based on the discussion of the $CH_3 + H_2$ reaction, predications can be made for other hydrogen exchange reactions. We always expect four phases, where the shape of the curvature peaks should reflect the polarizing power and polarizability of the reaction partners involved. If, for example the H in H_2 is replaced by a more polarizing agent such as F the cleavage peak should becomes broader and smaller.

Hydrogen Migration Reactions

The second example is a simple H-transfer reaction between a donor and an acceptor atom. In Figure 5, the curvature diagram of the 1,3 intramolecular H transfer in methanethioic O-acid yielding methanethioic S-acid (thioformic acid): S=C(H)OH → HSC(H)=O is shown.

The curvature diagram contains four curvature peaks K1 to K4, thus leading to a partitioning into four reaction phases. K1 relates to the OCS and HOC bending modes, K2 to the OH-stretching mode, K3 to the SH-stretching mode, and K4 to the OCS and the HSC bending mode. The reaction is initiated by deformation of the OCS skeleton (phase 1, light blue line, Figure 5), which first resists and then supports a curving of the reaction path. Bending supports a lengthening of the C=S bond (red line) and a bending of HOC (brown line). OCS and HOC bending initiates the start of OH bond cleavage (phase 2) and the forming of the SH bond. In phase 3, the SH bond formation is finalized. According to this mechanism, the energy barrier will increase if the ACB (A, B=O, S) heavy atom framework is made more rigid rather than by decreasing the H-acceptor capacity of B. The reverse reaction follows the same mechanistic pattern, where the heights of K2 and K3 can be related to the strength and stiffness of OH (higher) and SH bond (lower).

Symmetry Allowed Pericyclic Reactions

As a representative for a symmetry-allowed pericyclic reaction, the curvature diagram for the Diels–Alder reaction between ethene and butadiene is shown in Figure 6.[106]

The mechanism dissects into three reaction phases. In phase 1, electron spin-decoupling of the

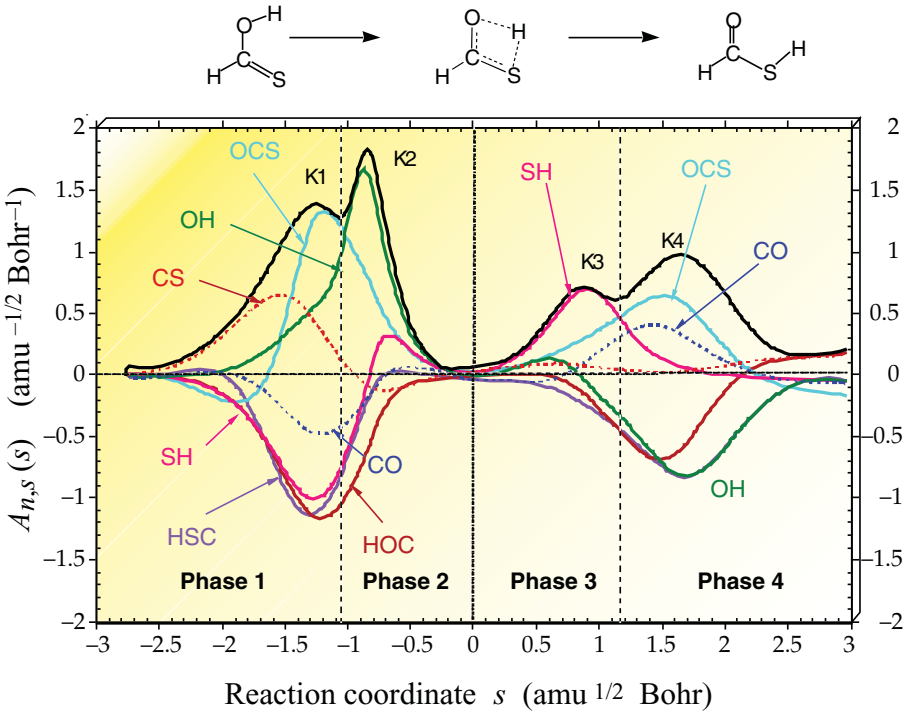

FIGURE 5 | Curvature diagram for the reaction: S=C(H)OH → HSC(H)=O. The scalar curvature $k(s)$ is given as a black line, the adiabatic curvature coupling coefficients $A_{n,s}(s)$ as colored lines. The transition state is located at $s = 0$ amu$^{1/2}$ Bohr. B3LYP/6-311G(d,p) calculations.[89]

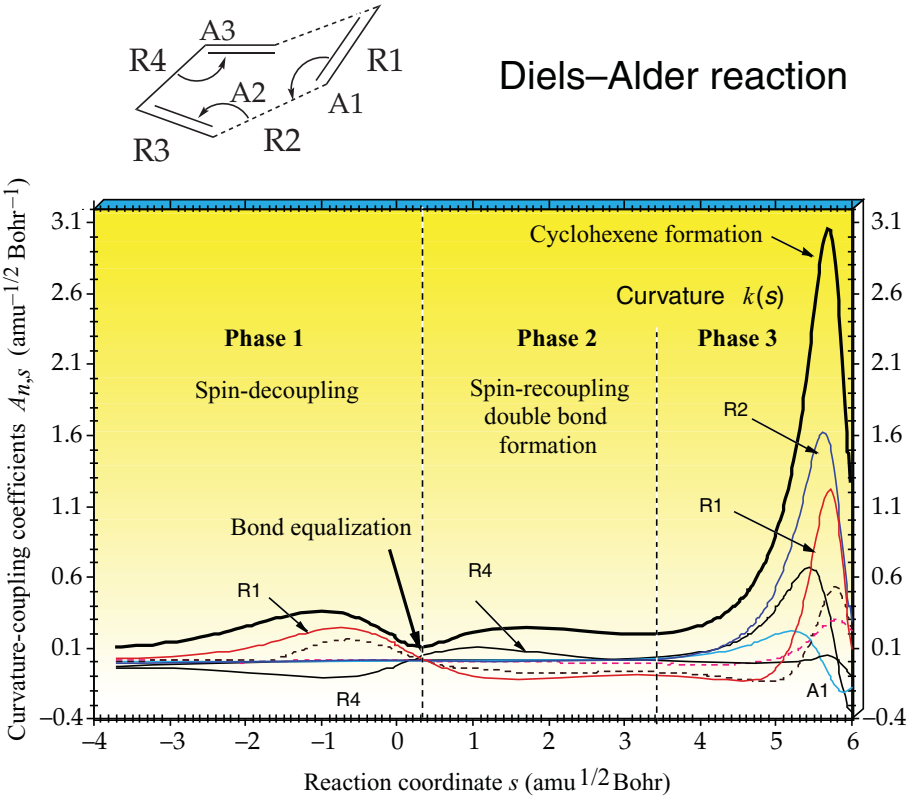

FIGURE 6 | Curvature diagram (top; bottom: enlarged) for a symmetry-allowed reaction: The Diels-Alder reaction, B3LYP/6-31G(d,p) calculations.[106]

π-bonds leads to bond equalization (R(CC) = 1.4 Å) shortly after the transition state at $s = 0$ amu$^{\frac{1}{2}}$ Bohr. In phase 2, spin recoupling results in the formation of a 2-butene structure with some 1,4-biradical character due to pyramidalization of the terminal CH_2 groups that has as a counterpart a similarly distorted ethene molecule (CC bond lengthened and CH_2 groups pyramidalized). In phase 3, far out in the exit channel, the two new CC bonds are formed. The curvature peaks in phases 1 and 2 close to the transition state are rather small and contain contributions from almost all of the adiabatic curvature coupling coefficients. Similar situations are found for other symmetry-allowed pericyclic reactions. A collective and smooth change of many internal coordinates requires less energy than the large change of just a few internal coordinates observed in symmetry-forbidden reactions.[107] Hence, the energy increase toward the transition state is moderate and a relatively low reaction barrier results. Also, typical of a symmetry-allowed reaction is the fact that close to the transition state a largely delocalized electron system with equalized heavy atom bonds is generated, denoted by a curvature minimum. This is in line with the Dewar–Evans–Zimmermann rules that compare the transition state of a symmetry-allowed pericyclic reaction with aromatic cyclopolyenes benefiting from electron delocalization.

Symmetry Forbidden Pericyclic Reactions, Hidden Intermediates

In Figure 7, the curvature diagram of the symmetry-forbidden cycloaddition reaction between ethene and HF is shown.[107]

Comparing Figures 6 and 7, it becomes obvious that the curvature pattern and hence the mechanism of symmetry-forbidden pericyclic reactions differ considerably from those of symmetry-allowed reactions. The cycloaddition reaction between ethene and HF is characterized by four curvature peaks and four reaction phases (van der Waals peak K1 and van der Waals phase are not shown) that indicate HF cleavage, CH bond formation (phases 2 + 3), and CF bond formation (phase 4).[107] The transient configuration of the reaction complex at $s = 2.7$ amu$^{\frac{1}{2}}$ Bohr resembles an ethyl cation separated from an F anion according to geometry and charge distribution.[107] If this transient structure is stabilized in a polar nonprotic solvent and/or F is exchanged for Br or I in the reaction complex, a real intermediate is obtained, which justifies to speak in the case of the gas phase reaction ethane and HF of the presence of a *hidden intermediate*.[89,107]

Reactions Without Barrier, Hidden Transition States

Figure 8 shows the curvature diagram $k(s)$, and three reaction phases of the chelotropic cycloaddition of $CH_2(^1A_1)$ to ethene yielding cyclopropane.[104]

The reaction proceeds without any barrier in a single, strongly exothermic step. Analysis of the reaction path curvature reveals a complicated mechanism comprising four different mechanistic phases (including the van der Waals phase not shown in Figure 8). Between the phases, *hidden transition state* (corresponding to a single CC bond formation) and *hidden intermediate* (corresponding to a trimethylene biradical) are located that can convert to real transition state or intermediate in the case of other carbenes, silylenes, or germylenes as was demonstrated for the reaction between difluorocarbene and ethene or the reaction between germylene and ethane.[104] In this way, the URVA analysis of the mechanism of the prototypical reaction $CH_2(^1A_1) + C_2H_4$ makes it possible to predict the mechanism of other chelotropic cycloaddition reactions in different environments thus opening up a new way of defining families of reactions with a similar curvature pattern and hence, similar mechanistic features.

An Alternative Approach: The Reaction Force Concept

While the URVA analysis is based on the analysis of the reaction path and its derivatives, Toro-Labbé and coworkers suggest elucidating the mechanism of a chemical reaction via the analysis of the derivative(s) of the energy along the reaction path leading to the *reaction force concept*.[110–113] The reaction force $f(s)$ is defined as the negative derivative of the potential energy $E(s)$ with respect to the reaction coordinate s,

$$f(s) = -\frac{\partial E(s)}{\partial s}, \tag{29}$$

whereas the second derivative of the potential energy $E(s)$ with respect to the reaction coordinate s, the curvature of $E(s)$ yields the *reaction force constant* $\kappa(s)$

$$\kappa(s) = \frac{\partial^2 E(s)}{\partial^2(s)} = -\frac{\partial f(s)}{\partial s}. \tag{30}$$

The minimum $f(s_\alpha)$ and maximum $f(s_\gamma)$ of $f(s)$ provide a partitioning of an elementary reaction into three distinct regions, the reactant region from s_A (starting point of the RP) to s_α (location of the reaction force minimum) and product region from s_γ (location of the reaction force maximum) to s_B (endpoint of the RP) characterized by structural

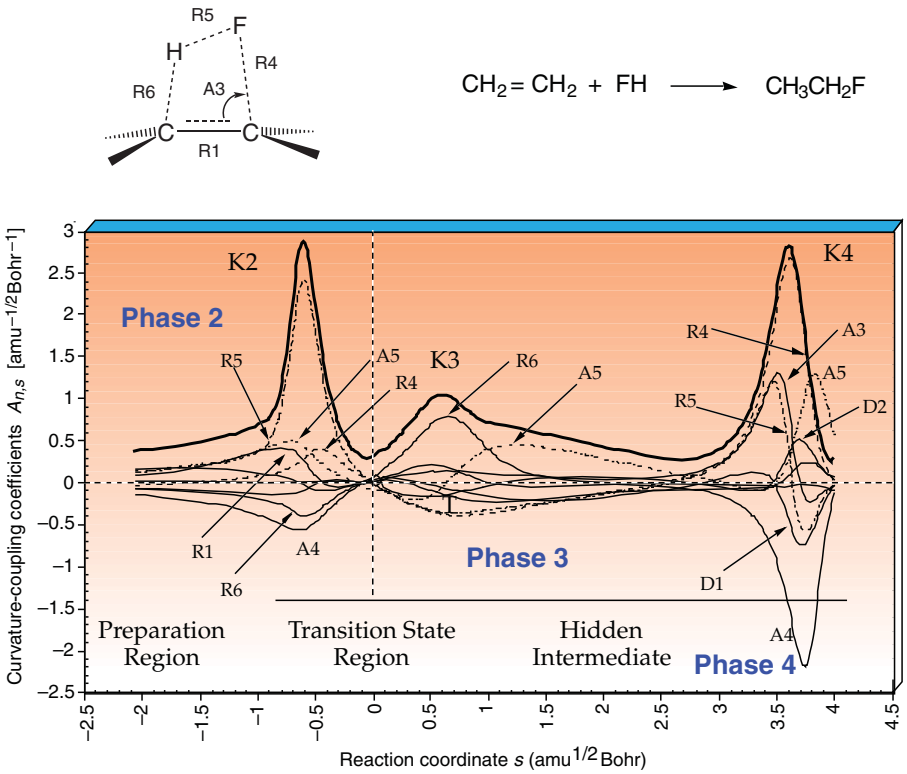

FIGURE 7 | Curvature diagram for a symmetry-forbidden reaction: The cycloaddition reaction of HF to ethane. The van der Waals phase is not shown. B3LYP/6-31G(d,p) calculations.[107]

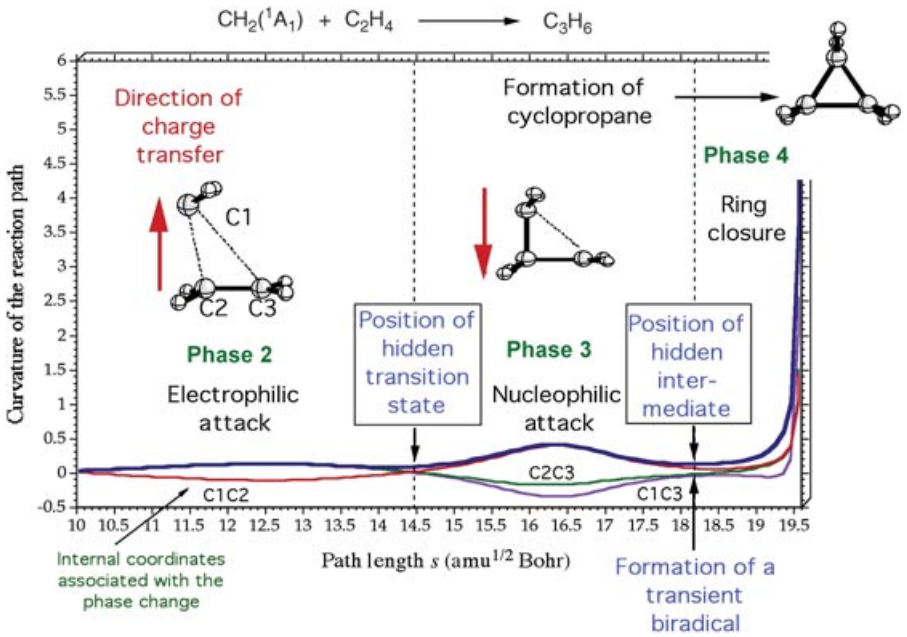

FIGURE 8 | Curvature diagram of the barrierless reaction $CH_2(^1A_1) + H_2C{=}CH_2 \rightarrow$ cyclopropane. Curvature (blue), some of the adiabatic curvature coupling coefficients (green, red, purple), and reaction phases (exception: van der Waals phase) are shown. B3LYP/6-31G(d,p) calculations.[104]

rearrangements embedding the transition state region from s_α to s_γ where the changes in the electronic properties of the reaction complex are assumed to take place. This region is characterized by negative reaction force constant $\kappa(s)$ values.

The study of different types of reactions[110–114] revels that certain characteristics can be assigned with each of the three regions. In the reactant region, structural changes such as bond stretching, rotations, and angle bending take place preparing the reaction complex for the actual reaction. The reaction force $f(s)$ is assumed to reflect any resistance to these changes and therefore becomes increasingly negative, i.e., retarding, until the minimum of $f(s)$ is reached at s_α, which is the point at which the preparation of the reaction complex is considered to be completed. In the second region between s_α and s_γ, the major portion of the transition toward products take place, which includes electronic changes accompanying bond breakages and bond formation. The reaction force includes now a growing driving component counteracting the resistance, which becomes dominant after point s_β, the location of the transition state. At s_γ, the maximum of $f(s)$, the third region begins dominated by structural relaxation of the reaction complex to reach the final product at s_B.

Changes of global and local electronic properties along the reaction coordinate and the whole electronic activity is rationalized in terms of polarization and transfer effects.[114] For this purpose, Toro-Labbé and coworkers analyze the derivative of the chemical potential $\mu(s)$ with respect to the reaction coordinate, the so-called reaction electronic flux (REF) $J(s)$

$$J(s) = -Q\frac{\partial \mu(s)}{\partial s}, \tag{31}$$

where Q is a transport coefficient.[114] The chemical potential is approximated via

$$\mu \approx \frac{1}{2}(\varepsilon_{\text{lumo}} + \varepsilon_{\text{hom}o}), \tag{32}$$

where $\varepsilon_{\text{lumo}}$ and $\varepsilon_{\text{hom}o}$are the energies of the lowest unoccupied and the highest occupied molecular orbitals, respectively.[115]

Regions with $J(s) > 0$ are associated with spontaneous changes of the electron distribution and regions with $J(s) < 0$ with nonspontaneous changes. $J(s)$ is decomposed into polarization and a transfer part,

$$J(s) = J_p(s) + J_t(s). \tag{33}$$

The flux part $J_p(s)$ describes the polarization of the electron density of the interacting fragments of the reaction complex induced by the reaction partners, and $J_t(s)$ describes intermolecular electronic transfer between the fragments of the reaction complex.

For a bimolecular reaction A + B, the polarization flux can be expressed as

$$\begin{aligned} J_p(s) &= J_A(s) + J_B(s) \\ &= -Q_A\frac{\partial \mu_A(s)}{\partial s} - Q_B\frac{\partial \mu_B(s)}{\partial s} \end{aligned} \tag{34}$$

with Q_A and Q_B being the transport coefficients associated with the polarization processes in A and B, μ_A and μ_B are the chemical potentials of the perturbed isolated molecules A and B along the RP.[114] Using Equations (33) and (34), the REF part due to electron transfer between A and B is given by

$$J_t(s) = J(s) - J_p(s). \tag{35}$$

As shown for the Schiff's base formation in the Maillard reaction,[114] the mechanism is characterized by interplay of both, polarization and transfer effects.

Toro-Labbé and coworkers complement the analysis of the REF by the study of local electronic properties such as Fukui functions[116] or electron population analysis schemes such as the natural bond orbital (NBO) analysis[117] to achieve a more detailed explanation of the mechanisms going beyond the three-region picture. However these quantities are model dependent, and therefore not always free from certain arbitrariness.

The URVA analysis and the reaction force analysis differ in some major point: The energy and all derivatives thereof are cumulative quantities that absorb all energy changes caused by geometry deformations and electronic structure adjustments of the reaction complex and accordingly lead to an overall picture. URVA avoids this problem by analyzing the reaction the complex and the path it traces in the course of the reaction via individual local modes thus obtaining both local and global rather than just global information. Local information added to the reaction force analysis results from concepts and model descriptions that are not necessarily consistent with that of the reaction force. In so far, it is not surprising that URVA detects any structural and electronic changes already in the van der Waals region. Structural changes always imply and are accompanied by electronic changes, and therefore it is problematic to separate them, i.e., invoking structural changes for the reaction and product region whereas electronic changes occur in the transition state region. It is more useful to distinguish between deformations of the reaction complex and the chemical processes of bond cleavage and bond formation. In URVA, these are distinguished and characterized by curvature

and curvature couplings. Via the curvature peaks and their decomposition into the adiabatic-coupling coefficients, details of mechanistically relevant features are displayed. The number of reaction phases defined by the curvature peaks varies with the number of chemical processes encountered in a chemical reaction rather than being restricted to three distinct regions: reactant, transition state, and product region. This is in line with recent findings of Toro-Labbé and coworkers[118] showing, that in the case of an asynchronous concerted mechanism being described by a potential energy profile with a shoulder before the transition state, a reaction force profile with more than two extrema results, going beyond the three-region picture.

The URVA concept can be applied to dissociation, recombination reactions, or in general, to barrierless reactions, as discussed above. In particular hidden transitions and hidden intermediates can be located which turn into real transition states and intermediates upon appropriate change of substituents and/or environment, as discussed above for the methylene addition to ethylene. The reaction force concept has been applied to bond dissociation and formation in diatomic molecules analyzing, an extended Rydberg potential energy function.[119] The analysis of the reaction force and reaction force constant leads to two distinct regions, the first involving the stretching or relaxation of the bond to be broken, followed by a transition between stretched molecule and the free atoms. This procedure may be extended to dissociation of a polyatomic molecule into two equivalent parts such as $C_2H_6 \rightarrow 2CH_3$, or a qualitative pseudodiatomic model for polyatomic bond dissociation,[120] but its general extension to asymmetric dissociation is not trivial. It is also not clear how the predictive power of the URVA analysis leading from a prototype to a family of related reactions (regardless whether these are single or multistep reactions, whether they proceed with or without a TS) can be realized within the reaction force concept.

However, this does not exclude that it may be useful to combine both concepts, which seem to be largely complementary, and to obtain in this way a more complete description of reaction mechanism. In this connection, however, care has to be taken that concepts are mixed that partly overlap or exclude each other.

CONCLUSION

The RPH is a powerful concept to investigate both the mechanism and the dynamics of a chemical reaction. The usefulness of the RPH for determining the dynamics of a chemical reaction has been demonstrated in many cases as shown in this article. Although developed in the 1980s, the RPH is a timeless concept, which always can be adjusted to recent developments either in theory and/or advances in computational methods. In particular, its future application to the calculation of rate constants in biological systems, including enzymatic reactions will definitely draw the attention of the computational chemistry community. Another strong potential of the RPH concept is the wealth of mechanistic information embedded in the RPH, which can be unraveled by URVA. Owing to the relationship between reaction complex and reaction path, analysis of the reaction path direction and curvature in terms of adiabatic vibrational modes leads to the dissection of the mechanism into reaction phases where the chemically important changes of the reaction complex take place defining the *fingerprints* for a certain reaction type. The analysis of the mechanism in terms of reaction phases for prototypical chemical reactions reveals that the chemical processes of bond breaking and forming can take place close to the transition state or far away in exit and entrance channel. The fate of a reaction is determined in the van der Waals phase. The adiabatic curvature coupling coefficients describing chemical processes can be related to bond strength as probed under the polarizing ability of an attacking reaction partner. Specific transient points along the reaction path associated with a curvature minimum can be converted to stationary points (transition state or minimum) if the reaction complex or the reaction conditions are changed in a specific way.

Current work aims at extending the URVA analysis to reactions in solution, homogenously or heterogeneously catalyzed reactions (reactions on surfaces), and reactions being import in biochemistry. The far-reaching goal is to fully understand the mechanisms of chemical reactions and to use this knowledge for the energy conserving production of new environment friendly materials.

APPENDIX

Derivation of Adiabatic Internal Coordinate Modes

The adiabatic mode vector $\mathbf{a}_n^Q$ (in terms of normal coordinates) for the nth adiabatic motion associated with the internal parameter q_n is expressed in terms of normal mode vectors $\mathbf{l}_\mu$ according to Equation (A.1)

$$\mathbf{a}_n^Q = \sum_{\mu}^{3K-L} \mathbf{l}_\mu \, Q_\mu^{(n)} \qquad \text{(A.1)}$$

with the expansion coefficients $Q_\mu^{(n)}$ describing $\mathbf{a}_n^Q$ under the constraint that the potential energy given in normal coordinates Q adapts a minimum while the internal coordinate displacement q_n is kept constant:

$$V(\mathbf{Q}) = \min \tag{A.2a}$$

$$q_n(\mathbf{Q}) = \text{const} = q_n^*. \tag{A.2b}$$

The potential energy V and the internal coordinate q_n depend on the normal coordinates according to Equations (A.3) and (A.4).

$$V(\mathbf{Q}) = \frac{1}{2}\sum_{\mu}^{3K\text{-}L} k_\mu Q_\mu^2 \tag{A.3}$$

$$q_n(\mathbf{Q}) = \sum_{\mu}^{3K\text{-}L} D_{n\mu}\, Q_\mu, \tag{A.4}$$

where k_μ is the force constant for normal mode d_μ and $D_{n\mu}$ is and element of the $\mathbf{D}$ matrix containing the normal mode vectors as column vectors expressed in internal coordinates.

Equation (29) is solved with the help of the method of Lagrange multipliers,

$$\frac{\partial V(\mathbf{Q})}{\partial Q_\mu} = [V(\mathbf{Q}) - \lambda(q_n(\mathbf{Q}) - q_n^*)] = 0 \tag{A.5}$$

leading to

$$\frac{\partial V(\mathbf{Q})}{\partial Q_\mu} = \lambda\left(\frac{\partial q_n(\mathbf{Q})}{\partial Q_\mu} - \frac{\partial q_n^*}{\partial Q_\mu}\right), \tag{A.6}$$

considering that $q_n(\mathbf{Q}) = q_n^*$ is constant. Inserting the expressions for $V(\mathbf{Q})$and $q_n(\mathbf{Q})$into Equation (A.6) results in

$$\frac{\partial}{\partial Q_\mu} = \frac{1}{2}\sum_{v}^{3K\text{-}L} k_v Q_v^2 = \lambda\frac{\partial}{\partial Q_\mu}\sum_{\rho}^{3K\text{-}L} D_{n\rho}\, Q_\rho \tag{A.7}$$

and

$$k_\mu = \lambda D_{n\mu}. \tag{A.8}$$

The solution of Equation (A.5) (which concerns internal parameter q_n) for the μth normal coordinate is

$$Q_\mu^{(n)} = \frac{D_{n\mu}}{k_\mu \lambda}, \tag{A.9}$$

where the superscript (n) of Q denotes a solution obtained under constraint (A.2b) for q_n. There is one such solution for each normal coordinate. When these solutions are used to express the displaced internal parameters $q_n{}^*$, one obtains

$$q_n^* = \sum_{\mu}^{3K\text{-}L} D_{n\mu}\, Q_\mu^{(n)} = \sum_{\mu}^{3K\text{-}L} \frac{D_{n\mu}^2}{k_\mu}\lambda, \tag{A.10}$$

which leads to the following expression for the Lagrange multiplier:

$$\lambda = \frac{1}{\sum_{\mu}^{3K\text{-}L} \frac{D_{n\mu}^2}{k_\mu}} q_n^*, \tag{A.11}$$

so that the following equation for the coefficients $Q_\mu^{(n)}$is obtained

$$Q_\mu^{(n)} = \frac{\frac{D_{n\mu}}{k_\mu}}{\sum_{\nu}^{3K\text{-}L} \frac{D_{n\nu}^2}{k_\nu}} q_n^*, \tag{A.12}$$

which means that the constraint for internal coordinate q_n leads to a change in the normal coordinates. The adiabatic internal mode $\mathbf{a}_n^Q$ for internal coordinate q_n expressed in terms of normal coordinates follows from (A.13):

$$Q_\mu^{(n)} = \left(\mathbf{a}_n^Q\right)_\mu\, q_n^*. \tag{A.13}$$

The AICoM $\mathbf{a}_n^Q$ can be transformed into an AICoM expressed in Cartesian coordinates, $\mathbf{a}_n$ with the help of the $\mathbf{L}$ matrix containing all normal modes $\mathbf{l}$ as column vectors

$$\mathbf{a}_n = \mathbf{L}\,\mathbf{a}_n^Q. \tag{A.14}$$

Hence Equations (A.13) and (A.14) completely determine the form of an AICoM.

Each AICoM possesses a force constant k_n^a

$$k_n^a = \mathbf{a}_m^\dagger\,\mathbf{f}\,\mathbf{a}_n \tag{A.15}$$

with the force constant matrix $\mathbf{f}$ in Cartesian coordinates, and a mass m_n^a

$$m_n^a = \frac{(\mathbf{b}_n^\dagger\mathbf{a}_n)^2}{\mathbf{b}_n^\dagger\mathbf{M}^{-1}\mathbf{b}_n} = G_{nn}, \tag{A.16}$$

where G_{nn} is an element of the Wilson $\mathbf{G}$ matrix, and vector $\mathbf{b}_n$ corresponds to the nth column of the Wilson $\mathbf{B}$ matrix, and the relation

$$\mathbf{b}_n^\dagger\mathbf{a}_n = 1 \tag{A.17}$$

holds, since the AICoMs are properly normalized.

With the AICoM force constant k_n^a and the AICoM mass m_n^a, it is straightforward to obtain the AICoM frequency ω_n^a

$$\omega_n^a = \left(\mathbf{a}_n^\dagger f\,\mathbf{b}_n G_{nn}\right)^{1/2} = \left(\frac{k_n^a}{m_n^a}\right)^{1/2}. \tag{A.18}$$

The force constant, frequency, and mass associated with a given AICoM for internal coordinate q_n fully characterize it. In this sense, the AICoMs are the dynamic counterparts of the internal coordinates, i.e.,

the latter are used to describe the equilibrium geometry of a molecule (static property) whereas the former describe the dynamic behavior of a molecule including the vibrational motions and the translational motion of a reaction complex during a reaction (dynamic behavior of a molecule).

ACKNOWLEDGMENTS

This work was financially supported by the National Science Foundation, Grant CHE071893. The author thanks SMU for providing computational resources. Fruitful discussions with Dieter Cremer are gratefully acknowledged as well as proofreading by Robert Kalescky.

REFERENCES

1. For an overview, see Dykstra CE, Frenking G, Kim KS, Scuseria GE, eds. *Theory and Applications of Computational Chemistry: The First Forty Years*. Amsterdam: Elsevier; 2005.
2. Piela L. *Ideas of Quantum Chemistry*. New York: Elsevier; 2007, chapter 14 and references cited therein.
3. Schlegel HB. Exploring potential energy surfaces for chemical reactions: an overview of some practical methods. *J Comp Chem* 2003, 24:1514–1527 and references cited therein.
4. Miller WH, Handy NC, Adams JE. Reaction path Hamiltonian for polyatomic molecules. *J Chem Phys* 1980, 72:99–112.
5. Kato S, Morokuma K. Potential energy characteristics and energy partitioning in chemical reactions: *ab initio* MO study of four-centered elimination reaction $CH_3CH_2F + CH_2 \rightarrow CH_2 + HF$. *J Chem Phys* 1980, 73:3900–3914.
6. Heidrich D, ed. *The Reaction Path in Chemistry: Current Approaches and Perspectives*. Dordrecht: Kluwer, 1995.
7. Kraka E. Reaction path Hamiltonian and its use for investigating reaction mechanism. In: Schleyer PvR, Allinger NL, Clark T, Gasteiger J, Kollman PA, Schaefer HF III, Schreiner PR, eds. *Encyclopedia of Computational Chemistry*. Chichester: John Wiley & Sons; 1998, 2437–2463.
8. Hofacker L. Quantentheorie Chemischer Reaktionen. *Z NaturforschA* 1963, 18:607–619.
9. Marcus RA. On analytical mechanics of chemical reactions. Quantum mechanics of linear collisions. *J Chem Phys* 1966, 45:4493–4449.
10. Marcus RA. On analytical mechanics of chemical reactions. Classical mechanics of linear collisions. *J Chem Phys* 1966, 45:4500–4504.
11. Marcus RA. Analytical mechanics of chemical reactions. 3. Natural collision coordinates. *J Chem Phys* 1968, 49:2610–2616.
12. Fukui K. The path of chemical-reactions—the IRC approach. *Acc Chem Res* 1981, 14:363–368.
13. Hougen JT, Bunker PR Johns JWC. Vibration-rotation problem in triatomic molecules allowing for a large-amplitude bending vibration. *J Mol Spectrosc* 1970, 34:136–172.
14. Page M, McIver JW Jr. On evaluating the reaction-path Hamiltonian. *J Chem Phys* 1988, 88:922–935.
15. Truhlar DG, Isaacson AD, Garrett BC. Generalized transition state theory. In: Baer M, ed. *Theory of Chemical Reaction Dynamics*. Boca Raton, FL: CRC Press; 1985, 65–173.
16. Fischer SF, Ratner MA. Theory of translational-vibrational energy-transfer for reactive collisions. *J Chem Phys* 1972, 57: 2769–2776.
17. Russegger P, Brickmann J. Quantum states of intramolecular nuclear motion with large amplitudes—pseudorotation of trigonal bipyramidal molecules. *J Chem Phys* 1975, 62:1086–1093.
18. For a recent summary, see: Garrett BC, Truhlar DG. Variational transition state theory. In: Dykstra CE, Frenking G, Kim KS, Scuseria GE, eds. *Theory and Applications of Computational Chemistry: The First Forty Years*. Amsterdam: Elsevier; 2005, 67–87.
19. Ruf BA, Miller WH. A new (Cartesian) reaction path model for dynamics in polyatomic systems, with application to H-atom transfer in malonaldehyde. *J Chem Soc, Faraday Trans 2* 1988, 84:1523–1534.
20. Natanson GA, Garrett BC, Truong TN, Joseph T, Truhlar DG. The definition of reaction coordinates for reaction path dynamics. *J Chem Phys* 1991, 94:7875–7892.
21. Chuang Y-Y, Truhlar DG. Reaction-path dynamics in redundant internal coordinates. *J Phys Chem A* 1998, 102:242–247.
22. Nguyen KA, Jackels CF, Truhlar DG. Reaction path dynamics in curvilinear internal coordinates including torsions. *J Chem Phys* 1996, 104:6491–6496.

23. Jackels CF, Gu Z, Truhlar DG. Reaction path potential and vibrational frequencies in terms of curvilinear internal coordinates. *J Chem Phys* 1995, 103: 3188–3201.
24. Wilson, EB Jr, Decius JC, Cross PC. *Molecular Vibrations: The Theory of Infrared and Raman Vibrational Spectroscopy*. New York: Dover; 1980.
25. Pulay P, Fogarasi G. Geometry optimization in redundant internal coordinates. *J Chem Phys* 1992, 96:2856–28606.
26. Okuno Y. A reaction path Hamiltonian described with quasirectilinear vibrational coordinates constructed from a nonlinear combination of curvilinear internal coordinates: formulation. *J Chem Phys* 2000, 113:3130–3135.
27. Okuno Y, Yokoyama S, Mashiko S. A reaction path Hamiltonian described with quasirectilinear vibrational coordinates constructed from a nonlinear combination of curvilinear internal coordinates: application to examination of the reaction $CH_4 + F \rightarrow CH_3 + HF$. *J Chem Phys* 2000, 113:3136–3140.
28. Eisenhart LP. *Riemannian Geometry*. Princeton, NJ: Princeton University Press; 1997.
29. Pavlov-Verevkin VB, Lorquet JC. Exit channel dynamics in barrierless unimolecular reactions: Criteria of vibrational adiabaticity. *J Chem Phys* 2005, 123:074324.
30. For a general discussion see, Smith IW. Vibrational adiabaticity in chemical reactions. *Acc Chem Res* 1990, 23:101–107.
31. Yan S, Wu, Y-T, Liu, K. Tracking the energy flow along the reaction path. *PNAS* 2008, 105:12667–12672 and references therein.
32. Miller WH. Reaction path models for polyatomic reaction dynamics–from transition state theory to path integrals. In: Clary DC, ed. *Theory of Chemical Reaction Dynamics*. Dordrecht: Reidel; 1986, 27–45.
33. Miller WH. Dynamical effects of symmetry along a reaction path: mode specificity in the unimolecular dissociation of formaldehyde. *J Am Chem Soc* 1983, 105:216–220.
34. Wardlaw DM. Reaction path Hamiltonian for the association reactions $CH_3 + H$ and $CH_3 + D$. *Can J Chem* 1992, 70:1892–1904.
35. Nauts, A, Chapuisat X. The description of molecular large-amplitude motions in terms of curvilinear coordinates associated with the reaction-path. *Chem Phys* 1983, 76:349–366.
36. Minichino C, Barone V. From concepts to algorithms for the characterization of reaction-mechanisms—H_2CS as a case-study. *J Chem Phys* 1994, 100:3717–3741.
37. Miller WH, Ruf BA, Chang Y-T. A diabatic reaction-path Hamiltonian. *J Chem Phys* 1988, 89:6298–6304.
38. Billing GD. Quantum-classical reaction path model for chemical reactions, I Theory and collinear atom-diatom case. *Chem Phys* 1984, 89:199–218.
39. Billing GD. Application of the reaction path method to the reaction $H + CH_4 \rightarrow H_2 + CH_3$. *Chem Phys* 2002, 277:325–340.
40. Baer M, Coletti C, Schatz GC, Toxvaerd S, Wang L. Scientific contributions of Gert Due Billing. *J Phys Chem A* 2004, 108:8554–8558.
41. Gonzales J, Gimenez X, Bofill JM. A restricted quantum reaction path Hamiltonian: theory, discrete variable representation propagation algorithm, and applications. *J Chem Phys* 2009, 131:054108.
42. Bohm D. A suggested interpretation of quantum theory in terms of "hidden" variables, Parts I and II. *Phys Rev* 1952 85:166–193.
43. Bladow LL, Stopera J, Thweatt WD, Page M. Mixed quantum-classical reaction path dynamics of HCL elimination from chloroethane. *J Phys Chem A* 2010, 114:4304–4312.
44. Miller WH, Shi S. Unified semiclassical perturbation and infinite order sudden approximation, with application to the reaction path Hamiltonian model. *J Chem Phys* 1981, 75:2258–2264.
45. Miller WH, Schwartz SD, Tromp JW. Quantum-mechanical rate constants for bimolecular reactions. *J Chem Phys* 1983, 79:4889–4898.
46. Yamashita K, Miller WH. 'Direct' calculation of quantum mechanical rate constants via path integral methods: application of the reaction path Hamiltonian, with numerical test for the $H + H_2$ reaction in 3D. *J Chem Phys* 1985, 82:5475–5484.
47. Miller WH. Reaction path models for polyatomic reaction dynamics–from transition state theory to path integrals. In: Clary DC, ed. *The Theory of Chemical Reaction Dynamics*. Boston, MA: Reidel; 1986, 27–45.
48. Lee S, Hynes JT. Solution reaction path Hamiltonian for reactions in polar solvents. I. Formulation. *J Chem Phys* 1988, 88:6853–8662.
49. Lee S, Hynes JT. Solution reaction path Hamiltonian for reactions in polar solvents. II. Applications. *J Chem Phys* 1988, 88:6863–8669.
50. Truhlar DG, Schenter GK, Garrett BC. Inclusion of nonequilibrium continuum solvation effects in variational transition-state theory. *J Chem Phys* 1993, 98:5756–5770.
51. Chuang, Y-Y, Truhlar DG. Nonequilibrium solvation effects for a polyatomic reaction in solution. *J Am Chem Soc* 1999, 121:10157–10167.
52. Ohmiya K, Kato S. Solution reaction path Hamiltonian based on reference interaction site model self-consistent field method: application to Menshutkin-type reactions. *J Chem Phys* 2003, 119:1605–1610.

53. Tenno S, Hirata F, Kato S. A hybrid approach for the solvent effect on the electronic-structure of a solute based on the RISM and Hartree–Fock equations. *Chem Phys Lett* 1993, 214:391–396.
54. Hu H, Kobrak MN, Xu C, Hammes-Schiffer S. Reaction path Hamiltonian analysis of dynamical solvent effects for a Claisen rearrangement and a Diels-Alder reaction. *J Phys Chem A* 2000, 104:8058–8066.
55. Lu Z, Yang W. Reaction path potential for complex systems derived from combined *ab initio* quantum mechanical and molecular mechanical calculations. *J Chem Phys* 2004, 121:89–100.
56. Hu H, Lu Z, Parks JM, Burger SK, Yang W. Quantum mechanics/molecular mechanics minimum free-energy path for accurate reaction energetics in solution and enzymes: sequential sampling and optimization on the potential of mean force surface. *J Chem Phys* 2008, 128:034105.
57. See, e.g., Manz J, Römelt J. Dissociative collinear reactions evaluated by S-matrix propagation along delves radial coordinate. *J Chem Phys Lett* 1981, 81:179–184.
58. Carrington T Jr, Miller WH. Reaction surface for the dynamics of reactions in polyatomic systems. *J Chem Phys* 1986, 84:3942–3949.
59. Carrington T Jr, Miller WH. Reaction surface description of intramolecular hydrogen atom transfer in malonaldehyde. *J Chem Phys* 1986, 84:4364–4370.
60. Miller WH, Schwartz S. System-bath decomposition of the reaction path Hamiltonian for polyatomic scattering: quantum perturbative treatment. *J Chem Phys* 1982, 77:2378–2382.
61. Tew DP, Handy NC, Carter S. A reaction surface Hamiltonian study of malonaldehyde. *J Chem Phys* 2006, 125:084313.
62. For a discussion of the MULTIMODE program combined with a RPH, see: Carter S, Handy NC. The vibrations of H_2O_2, studied by "multimode,' with a large amplitude motion. *J Chem Phys* 2000, 113;987–993.
63. Taketsugu T, Gordon MS. Reaction path Hamiltonian based on a reaction coordinate and a curvature coordinate. *J Chem Phys* 1996, 104:2835–2840.
64. Taketsugu T, Gordon MS. Dynamic reaction path analysis based on the intrinsic reaction coordinate. *J Chem Phys* 1995, 105:10042–10049.
65. Coletti, C, Billing GD. Reaction-volume approach to N-particle reactions: new optimization scheme for defining the reaction volume. *Phys Chem Chem Phys* 1999, 1:4141–4149.
66. Walet NR, Klein A. Reaction paths and generalized valley approximation. *J Chem Phys* 1889, 91:2848–2858.
67. Jang S, Rice SA. Reaction path analysis of the rate of unimolecular isomerization. *J Chem Phys* 1993, 99:9585–9590.
68. Fang J-Y, Hammes-Schiffer S. Time-dependent self-consistent-field dynamics based on a reaction path Hamiltonian I. Theory. *J Chem Phys* 1998, 108:7085–7099.
69. Fang J-Y, Hammes-Schiffer S. Time-dependent self-consistent-field dynamics based on a reaction path Hamiltonian II. *Numerical Tests* 1998, 109:7051–7063.
70. Hammes-Schiffer S. Quantum dynamics of multiple modes for reactions in complex systems. *Faraday Discuss. Chem Soc* 1998, 110: 391–406.
71. Meana-Paneda R, Truhlar GD, Fernandez-Ramos A. Least-action tunneling transmission coefficient for polyatomic reactions. *J Chem Theory Comput* 2010, 6:6–17.
72. Truhlar DG. Tunneling in enzymatic and nonenzymatic hydrogen transfer reactions. *J Phys Org Chem* 2010, 23:660–676.
73. Dybala-Defratyka A, Paneth P, Truhlar DG. In: Allemann RK, Scrutton NS, eds. *Enzyme Catalyzed Reactions*. Cambridge: Royal Society of Chemistry; 2009, 36–78.
74. Fehrensen B, Luckhaus D, Quack M, Willeke M, Rizzo T. *Ab initio* calculations of mode selective tunneling dynamics in $^{12}CH_3OH$ and $^{13}CH_3OH$. *J Chem Phys* 2003, 119:5534–5544.
75. Wang Y, Bowman JM. One-dimensional tunneling calculations in the imaginary-frequency rectilinear saddle-point normal mode. *J Chem Phys* 2008, 129:121103.
76. Luckhaus D. Large curvature tunneling on the reaction pat. *Phys Chem Chem Phys* 2008, 10:6215–6222.
77. Gonzales J, Gimenez X, Bofill JM. A reaction path-Liouville approach to the rate constant for polyatomic chemical reactions. *Phys Chem Chem Phys* 2002, 4:2921–2926.
78. Trofimov VV, Fomenko AT. Geometry of Poisson brackets and methods of Liouville integration of systems on symmetric spaces. *J Math Sci* 1987, 39:2683–2685.
79. Gonzales J, Gimenez X, Bofill JM. Algorithm to evaluate rate constants for polyatomic chemical reactions. I. Theory and computational details. *J Comp Chem* 2007, 28:2102–2110.
80. Gonzales J, Gimenez X, Bofill JM. Algorithm to evaluate rate constants for polyatomic chemical reactions. II. Applications. *J Comp Chem* 2007, 28:2111–2121.
81. Gonzales J, Gimenez X, Bofill JM. On the reaction path Hamiltonian for polyatomic molecules. *J Phys Chem A* 2001. 105:5022–5029.
82. Gonzales J, Gimenez X, Bofill JM. Generalized reaction-path Hamiltonian dynamics. *Theor Chem Acc* 2004, 112:75–83.

83. Gonzales J, Gimenez X, Bofill JM. A reaction path Hamiltonian defined on a Newton path. *J Chem Phys* 2002, 116:8713–8722.
84. Riedel J, Yan S., Liu K. Mode specificity in reactions of Cl with CH_2 stretch-excited CH_2D_2 (ν_1, $\nu_6 = 1$). *J Phys Chem A* 2009, 13: 14270–14276.
85. Duncan WT, Truong TN. Thermal and vibrational-state selected rates of the $CH_4 + Cl \rightarrow HCL + CH_3$ reaction. *J Chem Phys* 1995, 103:9642–9652.
86. Liu R, Ma S, Li Z. Theoretical study on the dynamic properties and state-selected rate constants of the reaction $CH(^4\Sigma_-) + H_2 \rightarrow CH_2(^3B_1) + H$. *Chem Phys Lett* 1994, 219;143–150.
87. Killelea D, Campbell VL, Shuman NS, Utz AL. Bond-selective control of a heterogeneously catalyzed reaction. *Science* 2008, 319;790–793.
88. Crim FF. Vibrational state control of bimolecular reactions: discovering and directing the chemistry. *Acc Chem Res* 1999, 32:877–884.
89. Kraka E, Cremer D. Computational analysis of the mechanism of chemical reactions in terms of reaction phases: hidden intermediates and hidden transition states. *Acc Chem Res* 2010, 43:591–601.
90. Konkoli Z, Kraka E, Cremer D. Unified reaction valley approach: mechanism of the reaction $CH_3 + H_2 \rightarrow CH_4 + H$. *J Phys Chem A* 1997, 101: 1742–1757.
91. Konkoli Z, Cremer D, Kraka E. Diabatic ordering of vibrational normal modes in reaction valley studies. *J Comp Chem* 1997, 18:1282–1289.
92. Cremer D, Kraka E. From molecular vibrations to bonding, chemical reactions, and reaction mechanism. *J Curr Org Chem*. 2010, 14:1524–1560.
93. Konkoli Z, Cremer D. A New way of analyzing vibrational spectra I. Derivation of adiabatic internal modes. *Int J Quant* 1998, 11:1–9.
94. Konkoli Z, Larsson, JA, Cremer D. A new way of analyzing vibrational spectra II. Comparison of Internal mode frequencies. *Int J Quant* 1998, 11:11–27.
95. Konkoli Z, Cremer D. A New way of analyzing vibrational spectra III. Characterization of normal vibrational modes in terms of internal vibrational modes. *Int J Quant* 1998, 11:29–40.
96. Konkoli Z, Larsson, JA, Cremer D. A new way of analyzing vibrational spectra IV. Application and testing of adiabatic modes within the concept of the characterization of normal modes. *Int J Quant* 1998, 11:41–55.
97. Kraka E, Cremer D. Characterization of CF bond with multiple-bond character: bond lengths, stretching force constants, and bond dissociation energies. *Chem Phys Chem* 2009, 10;689–698.
98. Cremer D, Larsson JA, Kraka E. New developments in the analysis of vibrational spectra: on the use of adiabatic internal vibrational modes. In: Parkanyi C, ed. *Theoretical and Computational Chemistry, Volume 5: Theoretical Organic Chemistry*. Amsterdam: Elsevier; 1998, 259–327.
99. Kraka E, Larsson JA, Cremer D. Generalization of the Badger rule based on the use of adiabatic vibrational modes. In: Grunenberg J, ed. *Vibrational Modes in Computational IR Spectroscopy*. New York: John Wiley & Sons; 2010, 105–149.
100. Quapp W. Gradient extremals and valley floor bifurcations on potential energy surfaces. *Theor Chim Acta* 1989, 75:447–460.
101. Quapp W, Hirsch, M, Heidrich D. Searching for saddle points of potential energy surfaces by following a reduced gradient. *J Comp Chem* 1998, 19:1087–1100.
102. See, e.g., Williams JH, Maggiora GM. Use and abuse of the distinguished-coordinate method for transition-state structure searching. *J Mol Struct: THEOCHEM* 1982, 6: 365–378.
103. Quapp W, Kraka E, Cremer D. Finding the transition state of quasi-barrierless reactions by a growing string method for Newton trajectories: application to the dissociation of methylenecyclopropene and cyclopropane. *J Phys Chem A* 2007, 111:11287–11293.
104. Joo H, Kraka E, Quapp W, Cremer, D. The mechanism of a barrierless reaction: hidden transition state and hidden intermediates in the reaction of methylene with ethene. *Mol Phys* 2007, 105:2697–2717.
105. Kraka E, Dunning TH, Jr. . Characterization of molecular potential energy surfaces: critical points, reaction paths and reaction valleys. In: Dunning TH Jr, ed. *Advances in Molecular Electronic Structure Theory: The Calculation and Characterization of Molecular Potential Energy Surfaces*. Greenwich: JAI Press; 1990, 129–173.
106. Kraka E, Wu A, Cremer D. The mechanism of the Diels–Alder reaction studied with the united reaction valley approach: mechanistic differences between symmetry-allowed and symmetry-forbidden reactions. *J Phys Chem A* 2003, 107:9008–9021.
107. Cremer D, Wu A, Kraka E. The Mechanism of the reaction $FH + H_2C{=}CH_2 \rightarrow H_3C{-}CFH_2$ investigation of hidden intermediates with the unified reaction valley approach. *Phys Chem Chem Phys* 2000, 3:674–687.
108. Kraka E, Cremer D. Mechanism and dynamics of organic reactions: 1,2-H shift in methylchlorocarbene. *J Phys Org Chem* 2002, 15:431–447.
109. Kraka E, Joo H, Cremer D. A stunning example for a spontaneous reaction with a complex mechanism: the vinylidene-acetylene cycloaddition reaction. *Mol Phys* 2010, 19–20:2667–2685.
110. Toro-Labbé A, Gutierrez-Oliva S, Murray JS, Politzer P. A new perspective on chemical and physical processes: the reaction force. *Mol Phys* 2007, 105:2619–2625.

111. Jaque P, Toro-Labbé A, Politzer P, Geerlings P. Reaction force constant and projected force constants of vibrational modes along the path of an intramolecular proton transfer reaction. *Chem Phys Lett* 2008, 456:135–140.

112. Toro-Labbé A, Gutierrez-Oliva S, Murray JS, Politzer P. The reaction force and the transition region of a reaction. *J Mol Model* 2009, 15:707–710.

113. Politzer P, Reimers JR, Murray JS, Toro-Labbé A. Reaction force and its link to diabatic analysis: a unifying approach to analyzing chemical reactions. *J Phys Chem Lett* 2010, 1:2858–2862.

114. Flores-Morales P, Gutiérrez-Oliva S, Silva S, Toro-Labbé A, The reaction electronic flux: a new descriptor of the electronic activity taking place during a chemical reaction. Application to the characterization of the mechanism of the Schiff's base formation in the Maillard reaction, *J Mol Struct: THEOCHEM* 2010, 943:121–126.

115. Parr RG, Yang W. *Density Functional Theory of Atoms and Molecules*. Oxford: Oxford University Press; 1994.

116. Contreras RR, Fuentealba P, Galván, Pérez P. A direct evaluation of regional Fukui functions in molecules. *Chem Phys Lett* 1999, 5–6:405–413.

117. Reed AE, Curtiss LA, Weinhold E. Intermolecular interactions from a natural bond orbital, donor acceptor viewpoint. *Chem Rev* 1988, 88:899–926.

118. Murray JS, Toro-Labbé A, Clark T, Politzer P. Analysis of diatomic bond dissociation and formation in terms of the reaction force and the position-dependent reaction force constant. *J Mol Model* 2009, 15:701–706.

119. Murray JS, Toro-Labbé A, Gutiérrez-Oliva S, Politzer P. Identification of pseudodiatomic behavior in polyatomic bond dissociation: reaction force analysis. *J Chem Phys* 2010, 132;154308–154314.

120. Labet V, Morell C, Toro-Labbé A, Grand A. Is an elementary reaction step really elementary? Theoretical decomposition of asynchronous concerted mechanisms. *Phys Chem Chem Phys* 2010, 12:4142–4151.

